C26 colon carcinoma [8]. Although the therapeutic effect depends on the type of cancer, we estimate that IL-12 concentrations of the order of tens of pg/ml are expressed at the tumor site using the present therapeutic system.

In conclusion, we demonstrated that the combination of Bubble liposomes and ultrasound effectively delivers the IL-12 gene into tumor tissue, and that local IL-12 production induces an immune response to the tumor cells. Therefore, the combination of Bubble liposomes and ultrasound could be a useful non-viral vector system in cancer gene therapy.

Acknowledgements

We thank Dr. Hiroshi Yamamoto (Department of Immunology, Graduate School of Pharmaceutical Sciences, Osaka University, Japan) for providing mIL-12 BIA/pBluescript II KS(−). We are grateful to Dr. Katsuro Tachibana (Department of Anatomy, School of Medicine, Fukuoka University, Japan) and Dr. Nobuki Kudo (Laboratory of Biomedical Instrumentation and Measurements, Graduate School of Information Science and Technology, Hokkaido University, Japan) for technical advice regarding the induction of cavitation with ultrasound exposure, to Dr. Yasuhiro Matsumura (Investigative Treatment Division, Research Center for Innovative Oncology, National Cancer Center Hospital East, Japan) for technical advice about cancer therapy, to Mr. Yasuyuki Shiono, Mr. Ryo Tanakadate, Mr. Kunihiko Matsuo, Mr. Ken Osawa and Ms. Motoka Kawamura (Department of Biopharmaceutics, School of Pharmaceutical Sciences, Teikyo University, Japan) for technical assistance, and to Mr. Yasuhiko Hayakawa, Mr. Takahiro Yamauchi and Mr. Kosho Suzuki (Nepa Gene Co., Ltd., Chiba, Japan) for technical advice about ultrasound exposure.

This study was supported by Grant-in-Aid for Young Scientists (B) from the Ministry of Education, Culture, Sports, Science and Technology of Japan, Grant-in-Aid for Scientific Research (A) and (B) from the Japan Society for the Promotion of Science, and Health and Labour Sciences Research Grants, Third Term Comprehensive Control Research for Cancer from the Ministry of Health, Labour and Welfare.

References

[1] U. Gubler, A.O. Chua, D.S. Schoenhaut, C.M. Dwyer, W. McComas, R. Motyka, N. Nabavi, A.G. Wolitzky, P.M. Quinn, P.C. Familletti, Coexpression of two distinct genes is required to generate secreted bioactive cytotoxic lymphocyte maturation factor, Proc Natl Acad Sci U S A 88 (1991) 4143–4147.
[2] S.F. Wolf, P.A. Temple, M. Kobayashi, D. Young, M. Dicig, L. Lowe, R. Dzialo, L. Fitz, C. Ferenz, R.M. Hewick, Cloning of cDNA for natural killer cell stimulatory factor, a heterodimeric cytokine with multiple biologic effects on T and natural killer cells, J Immunol 146 (1991) 3074–3081.
[3] M.J. Brunda, Interleukin-12, J Leukoc Biol 55 (1994) 280–288.
[4] C.L. Nastala, H.D. Edington, T.G. McKinney, H. Tahara, M.A. Nalesnik, M.J. Brunda, M.K. Gately, S.F. Wolf, R.D. Schreiber, W.J. Storkus, Recombinant IL-12 administration induces tumor regression in association with IFN-gamma production, J Immunol 153 (1994) 1697–1706.
[5] W.G. Yu, M. Ogawa, J. Mu, K. Umehara, T. Tsujimura, H. Fujiwara, T. Hamaoka, IL-12-induced tumor regression correlates with in situ activity of IFN-gamma produced by tumor-infiltrating cells and its secondary induction of anti-tumor pathways, J Leukoc Biol 62 (1997) 450–457.
[6] M.B. Atkins, M.J. Robertson, M. Gordon, M.T. Lotze, M. DeCoste, J.S. DuBois, J. Ritz, A.B. Sandler, H.D. Edington, P.D. Garzone, J.W. Mier, C.M. Canning, L. Battiato, H. Tahara, M.L. Sherman, Phase I evaluation of intravenous recombinant human interleukin 12 in patients with advanced malignancies, Clin Cancer Res 3 (1997) 409–417.
[7] J.P. Leonard, M.L. Sherman, G.L. Fisher, L.J. Buchanan, G. Larsen, M.B. Atkins, J.A. Sosman, J.P. Dutcher, N.J. Vogelzang, J.L. Ryan, Effects of single-dose interleukin-12 exposure on interleukin-12-associated toxicity and interferon-gamma production, Blood 90 (1997) 2541–2548.
[8] M.P. Colombo, M. Vagliani, F. Spreafico, M. Parenza, C. Chiodoni, C. Melani, A. Stoppacciaro, Amount of interleukin 12 available at the tumor site is critical for tumor regression, Cancer Res 56 (1996) 2531–2534.
[9] J.Q. Gao, T. Sugita, N. Kanagawa, K. Iida, Y. Eto, Y. Motomura, H. Mizuguchi, Y. Tsutsumi, T. Hayakawa, T. Mayumi, S. Nakagawa, A single intratumoral injection of a fiber-mutant adenoviral vector encoding interleukin 12 induces remarkable anti-tumor and anti-metastatic activity in mice with Meth-A fibrosarcoma, Biochem Biophys Res Commun 328 (2005) 1043–1050.
[10] Y. Gao, Z. Xu, S. Chen, W. Gu, L. Chen, Y. Li, Arginine-chitosan/DNA self-assemble nanoparticles for gene delivery: in vitro characteristics and transfection efficiency, Int J Pharm 359 (2008) 241–246.
[11] H. Hatakeyama, H. Akita, K. Kogure, M. Oishi, Y. Nagasaki, Y. Kihira, M. Ueno, H. Kobayashi, H. Kikuchi, H. Harashima, Development of a novel systemic gene delivery system for cancer therapy with a tumor-specific cleavable PEG-lipid, Gene Ther 14 (2007) 68–77.
[12] T. Montier, T. Benvegnu, P.A. Jaffres, J.J. Yaouanc, P. Lehn, Progress in cationic lipid-mediated gene transfection: a series of bio-inspired lipids as an example, Curr Gene Ther 8 (2008) 296–312.
[13] M. Morille, C. Passirani, A. Vonarbourg, A. Clavreul, J.P. Benoit, Progress in developing cationic vectors for non-viral systemic gene therapy against cancer, Biomaterials 29 (2008) 3477–3496.
[14] M. Fechheimer, J.F. Boylan, S. Parker, J.E. Sisken, G.L. Patel, S.G. Zimmer, Transfection of mammalian cells with plasmid DNA by scrape loading and sonication loading, Proc Natl Acad Sci U S A 84 (1987) 8463–8467.
[15] M.W. Miller, D.L. Miller, A.A. Brayman, A review of in vitro bioeffects of inertial ultrasonic cavitation from a mechanistic perspective, Ultrasound Med Biol 22 (1996) 1131–1154.
[16] C.M. Newman, T. Bettinger, Gene therapy progress and prospects: ultrasound for gene transfer, Gene Ther 14 (2007) 465–475.
[17] Z.P. Shen, A.A. Brayman, L. Chen, C.H. Miao, Ultrasound with microbubbles enhances gene expression of plasmid DNA in the liver via intraportal delivery, Gene Ther 15 (2008) 1147–1155.
[18] Y. Taniyama, K. Tachibana, K. Hiraoka, T. Namba, K. Yamasaki, N. Hashiya, M. Aoki, T. Ogihara, K. Yasufumi, R. Morishita, Local delivery of plasmid DNA into rat carotid artery using ultrasound, Circulation 105 (2002) 1233–1239.
[19] R. Suzuki, T. Takizawa, Y. Negishi, K. Hagisawa, K. Tanaka, K. Sawamura, N. Utoguchi, T. Nishioka, K. Maruyama, Gene delivery by combination of novel liposomal bubbles with perfluoropropane and ultrasound, J Control Release 117 (2007) 130–136.
[20] R. Suzuki, T. Takizawa, Y. Negishi, N. Utoguchi, K. Sawamura, K. Tanaka, E. Namai, Y. Oda, Y. Matsumura, K. Maruyama, Tumor specific ultrasound enhanced gene transfer in vivo with novel liposomal bubbles, J Control Release 125 (2008) 137–144.
[21] R. Suzuki, Y. Oda, N. Utoguchi, E. Namai, Y. Taira, N. Okada, N. Kadowaki, T. Kodama, K. Tachibana, K. Maruyama, A novel strategy utilizing ultrasound for antigen delivery in dendritic cell-based cancer immunotherapy, J Control Release 133 (2009) 198–205.
[22] T. Yamashita, S. Sonoda, R. Suzuki, N. Arimura, K. Tachibana, K. Maruyama, T. Sakamoto, A novel bubble liposome and ultrasound-mediated gene transfer to ocular surface: RC-1 cells in vitro and conjunctiva in vivo, Exp Eye Res 85 (2007) 741–748.
[23] Y. Negishi, Y. Endo, T. Fukuyama, R. Suzuki, T. Takizawa, D. Omata, K. Maruyama, Y. Aramaki, Delivery of siRNA into the cytoplasm by liposomal bubbles and ultrasound, J Control Release 132 (2008) 124–130.
[24] K. Un, S. Kawakami, R. Suzuki, K. Maruyama, F. Yamashita, M. Hashida, Enhanced transfection efficiency into macrophages and dendritic cells by the combination method using mannosylated lipoplexes and Bubble liposomes with ultrasound exposure Hum Gene Ther. (2009) In press.
[25] M. Hashimoto, O. Niwa, Y. Nitta, M. Takeichi, K. Yokoro, Unstable expression of E-cadherin adhesion molecules in metastatic ovarian tumor cells, Jpn J Cancer Res 80 (1989) 459–463.
[26] Y. Okada, N. Okada, S. Nakagawa, H. Mizuguchi, M. Kanehira, N. Nishino, K. Takahashi, N. Mizuno, T. Hayakawa, T. Mayumi, Fiber-mutant technique can augment gene transduction efficacy and anti-tumor effects against established murine melanoma by cytokine-gene therapy using adenovirus vectors, Cancer Lett 177 (2002) 57–63.
[27] C. Fillat, M. Carrio, A. Cascante, B. Sangro, Suicide gene therapy mediated by the Herpes Simplex virus thymidine kinase gene/Ganciclovir system: fifteen years of application, Curr Gene Ther 3 (2003) 13–26.
[28] X.H. Shi, Z.Y. Liang, X.Y. Ren, T.H. Liu, Combined silencing of K-ras and Akt2 oncogenes achieves synergistic effects in inhibiting pancreatic cancer cell growth in vitro and in vivo, Cancer Gene Ther 16 (2009) 227–236.
[29] M. Nogawa, T. Yuasa, S. Kimura, M. Tanaka, J. Kuroda, K. Sato, A. Yokota, H. Segawa, Y. Toda, S. Kageyama, T. Yoshiki, Y. Okada, T. Maekawa, Intravesical administration of small interfering RNA targeting PLK-1 successfully prevents the growth of bladder cancer, J Clin Invest 115 (2005) 978–985.
[30] C.W. Beh, W.Y. Seow, Y. Wang, Y. Zhang, Z.Y. Ong, P.L. Ee, Y.Y. Yang, Efficient delivery of Bcl-2-targeted siRNA using cationic polymer nanoparticles: down-regulating mRNA expression level and sensitizing cancer cells to anticancer drug, Biomacromolecules 10 (2009) 41–48.
[31] M. Folini, M. Pennati, N. Zaffaroni, RNA interference-mediated validation of genes involved in telomere maintenance and evasion of apoptosis as cancer therapeutic targets, Methods Mol Biol 487 (2009) 303–330.
[32] S. Lehrman, Virus treatment questioned after gene therapy death, Nature 401 (1999) 517–518.
[33] C.C. Conwell, L. Huang, Recent advances in non-viral gene delivery, Adv Genet 53PA (2005) 1–18.
[34] N. Kanagawa, J.Q. Gao, Y. Motomura, T. Yanagawa, Y. Mukai, Y. Yoshioka, N. Okada, S. Nakagawa, Antitumor mechanism of intratumoral injection with IL-12-expressing adenoviral vector against IL-12-unresponsive tumor, Biochem Biophys Res Commun 372 (2008) 821–825.

Journal of Electron Microscopy Advance Access published November 11, 2009

Journal of Electron Microscopy: 1–10 (2009)
doi: 10.1093/jmicro/dfp056

Physical: Full-length—Experimental

Morphological study of acoustic liposomes using transmission electron microscopy

Tetsuya Kodama[1,*], Noriko Tomita[1,5], Sachiko Horie[1], Nicolas Sax[1], Hiroko Iwasaki[1], Ryo Suzuki[2], Kazuo Maruyama[2], Shiro Mori[3] and Fukumoto Manabu[4]

[1]Graduate School of Biomedical Engineering, Tohoku University, 2-1 Seiryo, Aoba, Sendai, 980-8575, Japan, [2]Department of Biopharmaceutics, School of Pharmaceutical Sciences, Teikyo University, 1091-1 Suwarashi, Sagamiko, Sagamihra, Kanagawa, 229-0195, Japan, [3]Department of Oral Health Science, Tohoku University Hospital, 1-1 Seiryo, Aoba, Sendai, 980-8574, Japan and [4]Institute of Development, Aging and Cancer, Tohoku University, 4-1 Seiryo, Aoba, Sendai, 980-8575, Japan
[5]Present address: Institute of Fluid Science, Tohoku University, 2-1-1 Katahira, Aoba, Sendai, 980-8577, Japan
*To whom correspondence should be addressed. E-mail: kodama@bme.tohoku.ac.jp

Abstract Sonoporation is achieved by ultrasound-mediated destruction of ultrasound contrast agents (UCA) microbubbles. For this, UCAs must be tissue specific and have good echogenicity and also function as drug carriers. Previous studies have developed acoustic liposomes (ALs), liposomes that encapsulate phosphate buffer solution and perfluoropropane (C_3F_8) gas and function as both UCAs and drug carriers. Few studies have examined the co-existence of gas and liquid in ALs. This study aims to elucidate AL structure using TEM. The size, zeta potential and structure of ALs were compared with those of two other UCAs, human albumin shell bubbles (ABs; Optison) and lipid bubbles (LBs). ABs and LBs encapsulate the C_3F_8 gas. Particle size was measured by dynamic light scattering. The zeta potential was determined by the Smoluchowski equation. UCA structure was investigated by TEM. ALs were ~200 nm in size, smaller than LBs and ABs. ALs and LBs had almost neutral zeta potentials whereas AB values were strongly negative. The negative or double staining TEM images revealed that ~20% of ALs contained both liquid and gas, while ~80% contained liquid alone (i.e. nonacoustic). Negative staining AB images indicated electron beam scattering near the shell surface, and albumin was detected in filament form. These findings suggest that AL is capable of carrying drugs and high-molecular-weight, low-solubility gases.

Keywords nanobubbles, drug delivery system, sonoporation, ultrasound contrast agent, cavitation

Received 25 June 2009, accepted 5 October 2009

Introduction

Ultrasound contrast agents (UCAs) are nano/microbubbles that contain air or a high-molecular-weight, low water-solubility gas (e.g. C_3F_8, C_4F_{10} and SF_6) encapsulated in a lipid or albumin shell [1–6]. The diameters of UCAs vary from 100 nm to 10 μm and their behavior primarily depends on the ultrasound characteristics. The behavior of UCAs is described by an equation of motion that consists of external force, viscosity and stiffness terms [7]. When the external force is small, i.e. ultrasound pressure is small, UCAs undergo small volumetric oscillation (linear). With increasing ultrasound pressures, the amplitude of volumetric oscillation increases and

oscillation becomes aperiodic (nonlinear), resulting in destruction of UCAs [1,8].

Drug delivery via sonoporation using ultrasound and UCAs is a technique used for diagnosis and treatment [1,8] and is based on bubble destruction modes. During sonoporation, primary UCAs and subsequent bubble cavitation generated by the collapse of the UCAs induce mechanical forces such as liquid jets and shock waves [8]. These forces interact with the surrounding cells, resulting in the permeation of exogenous molecules into cells [1,8]. Sonoporation is a noninvasive, nonimmunogenic and tissue-specific procedure that has been used to treat cancer and many other diseases [1,3,9]. However, the efficiency of molecular delivery is relatively low; therefore, it has not been recognized as a clinically valuable approach. One strategy towards improving the efficiency of molecular delivery is to develop UCAs that are tissue-specific and that can function as drug carriers. Suzuki *et al.* [9] developed a novel form of liposome containing the C_3F_8 gas and phosphate buffer solution and demonstrated that it functions as an acoustic liposome (AL) applicable to a nonvirus molecular delivery system [5,6]. The liposome surface was covered with polyethyleneglycol (PEG); therefore, it was assumed that this molecule would not be incorporated by the reticuloendothelial system, thereby allowing a longer retention in the blood [10]. In addition, the tumor-targeting potential and drug-carrying capability are significantly improved by conjugating PEG with ligands specific for the target tissue and by producing bubbles with diameters of <100 nm, which allows for enhanced permeability and retention (EPR) effects [11,12]. These studies concluded that the liposome would be acoustic due to the differences between ultrasound backscatter intensities in the presence/absence of ultrasound. However, the coexistence of gas and liquid in the liposome has not been examined, neither have its size and structure been discussed.

The present study investigated the size, zeta potential and structure of ALs and compared these values with those of two other types of UCAs: a single human albumin shell (ABs; Optison) and lipid bubbles (LBs). Both UCAs encapsulated the C_3F_8 gas, which was identical to the liposome gas. Transmission electron microscopy (TEM) was used to assess the structure of UCAs, and the TEM images were obtained using either negative or double staining. The TEM findings will be used as parameters to evaluate biodistribution, safety and efficacy of micro/nanoparticulate systems.

Methods

Nano/microbubble preparation

Three types of UCA—ABs ($5.0–8.0 \times 10^8$ bubbles mL^{-1}; Optison™, Amersham Health Plc, Oslo, Norway), LBs and ALs—were used. LBs were created in an aqueous dispersion of 2 mg mL^{-1} 1,2-distearoyl-sn-glycero-phosphatidylcholine (DSPC) (Avanti Polar Lipids, Alabaster, AL, USA) and 1 mg mL^{-1} polyethylene glycol (PEG) distearate (Sigma-Aldrich) using a 20 kHz stick sonicator (130 W, Vibra Cell, Sonics & Materials Inc., Danbury, CT, USA) at 50% amplifying strength for 1 min, in the presence of C_3F_8 gas in a sterilized 7 mL Bijou vial [8,13,14]. The vial cap has two openings that serve as a gas inlet and outlet. During sonication, the C_3F_8 gas was kept under the condition of inflow and outflow through the openings. The LB concentration was 3.4×10^8 bubbles mL^{-1} [13]. ALs were prepared by modifying the protocol of Suzuki *et al.* [9]. First, DSPC (NOF Co., Tokyo, Japan) and 1,2-distearoyl-sn-glycero-3-phosphatidyl-ethanolamine-methoxy-polyethyleneglycol (DSPE-PEG2000-OMe) (NOF Co.) (94:6 [mol/mol]) were dissolved in 10 mL of 9:1 (v/v) chloroform/methanol. Next, 5 mL of phosphate-buffered saline (PBS) without Mg^{2+} and Ca^{2+} (pH 7.2 at room temperature, Sigma) was added to the solution. The solution was then sonicated using a 20 kHz stick sonicator (Sonics & Materials). Liposomes were obtained by reverse phase evaporation at 65°C. The organic solvent was completely removed, and the size of the liposomes was adjusted to <100 nm using extruding equipment (Northern Lipids Inc., Vancouver, BC, Canada) with three sizing filters (pore sizes: 100, 200 and 600 nm) (Nuclepore Track-Etch Membrane, Whatman plc, UK). The resulting liposomes were passed through a 0.45 μm pore size filter (MILLEX HV filter unit, Durapore polyvinylidine-difluoride (PVDF) membrane, Millipore Corporation, MA, USA) for sterilization. Lipid concentration was measured using the Phospholipid *C*-test Wako (Wako Pure Chemical Industries, Ltd, Osaka, Japan). To produce AL, a

liposome suspension of 1 mL (lipid concentration: 1 mg mL^{-1}) was sonicated using a bath sonicator (42 kHz, 100 W; Bransonic 2510J-DTH, Branson Ultrasounics Co., Danbury, CT, USA) and a 20 kHz stick sonicator (130 W, Sonics & Materials, Inc.) at 50% amplifying strength for 1 min, in the presence of C_3F_8 in a sterilized 7 mL Bijou vial, as described above.

Dark field microscopy

Immediately after sonication, 20 μL drops of either AL or LB were put on a glass cover and were observed under an inverted microscope (IX81, Olympus, Tokyo, Japan) equipped with an illuminator (Darlkite Illuminator, Micro Video Instruments, Avon, MA , USA).

Echogenicity measurement

The air inside the 5 mL vials containing 1 mL of liposome suspension (lipid concentration: 1 mg mL^{-1}) sealed with a rubber cap together with an aluminium jacket was replaced with 12 mL of air or C_3F_8 gas and supercharged with another 12 mL of each gas. The suspension in the vial was sonicated in a bath sonicator (Branson Ultrasounics) for 2 min. The suspension was transferred to a 7 mL Bijou vial and further sonicated by a 20 kHz sonicator (Sonics & Materials) at 50% amplifying strength for 1 min while 5 mL of each gas was injected at a rate of 300 mL h^{-1} using a syringe pump (model KDS 100, KD Scientific, Holliston, MA, USA). Four milliliters of a 40-fold dilution with PBS were added to a well of a 6-well plate and the B-mode image was acquired with a high-frequency ultrasound imaging system with a center frequency of 55 MHz (VEVO 770, Visualsonics Inc., Toronto, Canada). The grayscale histogram of a selected ROI was measured using the implemented software of the US imaging system. The ROI circle was set to 1.00 mm^2, 1 mm above the bottom of the well.

Size and zeta potential

The size and zeta potentials of the bubbles were measured using a zeta potential & particle size analyzer (zeta potential range: −200 to +200 mV, particle size/distribution range: 0.6 nm to 7 μm, laser source: laser diode (660 nm), ELSZ-2, Otsuka Electronics, Osaka, Japan). The size was measured using the dynamic light scattering. The zeta potential was automatically calculated on the basis of the electrophoretic mobility using the Smoluchowski equation: $\zeta = 4\pi\eta u/\varepsilon$, where ζ is the zeta potential, u is the electrophoretic mobility and η and ε are the viscosity and dielectric constant of the solvent, respectively. The Smoluchowski equation is applicable to a solid surface on which a surface-charge layer exits and electrolyte ions do not penetrate through the surface, i.e. hard particles [15]. In the present study, the three types of bubbles were assumed to be hard particles. The bubble solutions were diluted in PBS to $\sim 10^7$ bubbles mL^{-1} at room temperature (21–23°C). The average values of the sizes and zeta potentials were calculated using four to nine independent measurements on each sample.

TEM

Either negative or double staining was used for AL. Negative staining was used for LB and AB. The stained samples were examined with a JEM-2000EX operated at 100 kV (JEOL Datum, Tokyo, Japan) at the Hanaichi UltraStructure Research Institute, Aichi, Japan; or with a H-7600 operated at 80 kV (Hitachi Tokyo, Japan) at Tohoku University, Sendai, Japan. For the negative staining, a 400-mesh grid (EM fine-grid F-400, Nisshin EM Co., Tokyo, Japan) with a carbon support film (10–20 nm in thickness) was used, and was given a hydrophilic treatment. Samples were stained at either room temperature or at 80°C. For the former case, a drop of sample solution, distilled water and phosphotungstic acid (Merck, Tokyo, Japan) were put on a parafilm (Pechiney Plastic Packaging Co., Menasha, WI, USA). The grid was put into the sample drop (30 s), then in a distilled water drop for washing (10 s) and finally in a phosphotungstic acid drop for staining (10 s). Any excess solution was removed with filter paper. For the latter case, a parafilm was floated on water heated at 80 °C, and the procedure outlined above was then followed. For the double staining, an AL solution generated in the presence of C_3F_8 in a sterilized 7 mL vial was immediately added to 1 mL of 2% agarose (Cambrex Bio Science Rockland, Inc., Rockland, USA) to obtain a stable solution that did not release gas. Then, the AL solution was mixed with the same amount of

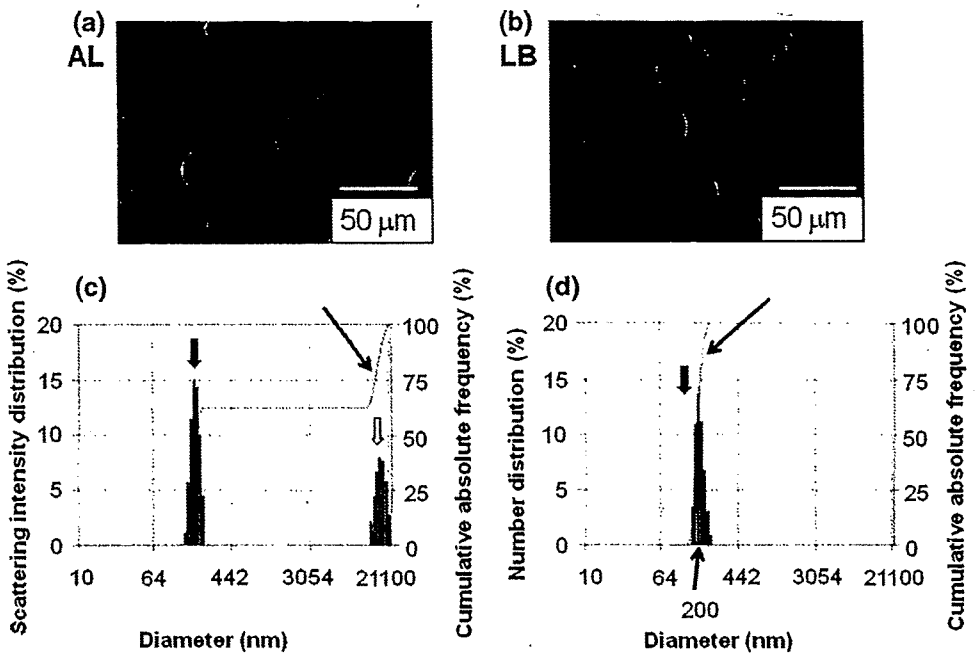

Fig. 1. Dark field images of ALs and LBs and size distribution of ALs. (a) AL dark field image. (b) LB dark field image. (c) Scattering intensity distribution (%) and cumulative absolute frequency (%) of ALs, measured using dynamic light scattering. There are two peaks indicating diameters of ~200 nm (⇓) and 15 700 nm (⇩). (d) Number distribution (%) and cumulative absolute frequency (%) of AL, measured by dynamic light scattering. Approximately 100% of ALs were ~200 nm in diameter (⇓). ALs with diameters exceeding a few micrometers accounted for <0.01%. The arrows (↓) in (c) and (d) indicate the line of the cumulative absolute frequency (%).

2% osmium tetroxide solution, and was fixed at 4°C for 6 h. Dehydration in an ethanol series (50–100%) at room temperature followed, and the solution was embedded in an EPON812 resin mixture at 60°C for 48 h. Thin sections were obtained using an ultramicrotome (Power Tome XL, RMC, Boekeler Instruments, Tucson, AZ, USA). They were stained with 2% uranyl acetate (Merck) for 15 min, washed with rinse solution and were finally stained with a lead stain solution (Sigma, Tokyo, Japan) for 5 min. Histogram of the absolute frequency distribution was obtained from 10 TEM images. The diameter of each AL was measured with rulers.

Brightness analysis

Two sets of TEM images (ALs, and non-gas-containing liposomes [LSs]) were analyzed to assess the average brightness value of the inside of each kind of liposome. The inner area of each liposome on the images was individually selected and its mean brightness value obtained by the ImageJ software (Rasband, W. S., Image J, U. S. NIH, Bethesda, MD, USA, http://rsb.info.nih.gov/ij/, 1997–2009.). For each image, a brightness value of the background was measured and used for normalization. Overstained areas were left out for both types of measurements. Relative brightness values (measured mean brightness/background brightness) were obtained for 106 LSs and 83 ALs.

Statistical analysis

All measurements were represented as either mean ± SD (standard deviation) or SEM (standard error of the mean). Statistical analysis was performed by using Student's *t*-test. Difference with $P < 0.05$ was considered significant. The statistical analysis was performed using Excel 2000 (Microsoft, USA) with the add-in software Statcel 2 [16].

Results

First, the data obtained for ALs and LBs using dark light microscopy were examined, given that both have similar membrane components (Fig. 1a and b). Figure 1a shows that each AL was captured clearly. ALs with a diameter of up to 30 μm existed. Figure 1c shows the percentage of scattering intensity distribution and cumulative absolute frequency of ALs. Two peaks were observed indicating diameters of ~200 nm and 15 700 nm. Figure 1d shows the

Table 1. Bubble characteristics

Nano/microbubble	Shell	Gas	[a]Size (nm)	[b]Zeta potential (mV)
AL	DSPC/DSPE-PEG2000	Perfluoropropane	199 ± 84.4 ($n = 8$)	-2.1 ± 0.9 ($n = 4$)
LB	DSPC/PEG	Perfluoropropane	1222 ± 442.7 ($n = 9$)	-4.2 ± 1.3 ($n = 5$)
AB (Optison)	Albumin	Perfluoropropane	1689 ± 299.8 ($n = 4$)	-40 ± 6.9 ($n = 4$)

[a]Size was measured using dynamic light scattering. Approximately 100% of ALs were ~200 nm in diameter. ALs with diameters larger than a few micrometers accounted for <0.01% (see Fig. 1). Further, 90% of the LBs were ~1200 nm in diameter (data not shown).
[b]The zeta potential was calculated using the Smoluchowski equation.
Values are represented as mean ± SD.

number distribution (%) and cumulative absolute frequency (%), which have been converted from Fig. 1c. Results show that most ALs have diameters of ~200 nm, while ALs with diameters exceeding a few micrometers accounted for <0.01% (Fig. 1c and d). Figure 1b shows the overall LB view. Although large bubbles were visible, the tiny bubbles that were observed in Fig. 1a were not detected in Fig. 1b. The mean diameters for the ALs, LBs and ABs are summarized in Table 1, with AL diameter being one digit smaller than that of the LBs and ABs.

To confirm that the C_3F_8 gas was actually encapsulated by the AL shell, we measured the echogenicity of liposomes sonicated in the presence of either atmospheric air or C_3F_8 gas. Figure 2a shows characteristics of liposomes under either atmospheric air or C_3F_8 gas. Photos show that liposome suspension sonicated in the presence of C_3F_8 is cloudier than that of air and original liposome suspension (NONE). Next we measured echogenicity of each bubble by the method indicated in Fig. 2c. The US B-mode images show that liposome sonicated in the presence of the C_3F_8 gas have a high echogenicity. This tendency is confirmed by the brightness histogram of the liposome sonicated in the presence of the C_3F_8 gas that displays a shift to the right of the brightness levels compared to that with air. Figure 2b indicates the difference of brightness value between liposome sonicated in the presence of either atmospheric air or C_3F_8 gas. The values were normalized by that of NONE. There is a highly significant difference between them ($P < 0.01$).

The zeta potential is one of the primary parameters indicative of drug delivery efficiency, since it informs about dispersivity, aggregability and mutual interaction inside the colloidal suspension. Zeta potential values are summarized in Table 1. ALs and LBs possessed neutral values since neutral lipid phosphatidylcholine was the primary component of their shells and the PEG distributed on their shell surfaces is a nonelectrolyte, water-soluble polymer. ABs had a strong negative charge, indicating that the AB colloid is the most stable of the three bubble types.

Next, ALs were stained using negative staining, and their structures were examined by TEM (Fig. 3). In general, when a lipid bilayer is negatively stained, the stain solution penetrates the lipid bilayer. Existence of gas within certain areas of ALs will prevent that area from being stained effectively, resulting in a reduction in net electron density in that area. The black arrows in Fig. 3a and b indicate the presence of gas within the ALs. Decreased electron density in the central area was apparent in 69 out of 345 ALs, i.e. 20%. The shape of LBs (Fig. 3c and d) was not always spherical as compared to the shapes of ALs. A significant decrease in electron density was not observed in the interior making it difficult to determine whether gas existed in the LB. Figure 3d shows that some LBs had a bag configuration suggesting that an LB may potentially contain both gas and liquid. The AB shell structure caused strong electron beam scattering around the shell (Fig. 3e). As shown in the magnified figure (Fig. 3f), albumin was observed in filament form (indicated by the black arrow), with the layer being several hundred nanometers thick. The interior gas was assumed to be packed in a stable manner and covered with the thick albumin shell. The internal electron density was relatively low, indicating the existence of gas. Figure 4 shows the histogram of the absolute frequency distribution obtained from 10 TEM micrographs. The maximum value was obtained within the class interval of 91–120 nm. This value was about half that measured with dynamic light scattering (see Table 1). Figure 5 shows the distribution of relative brightness values in original liposomes (LSs) and ALs. The statistical distribution of ALs is slightly shifted to relative brightness values closer to 1 compared to the

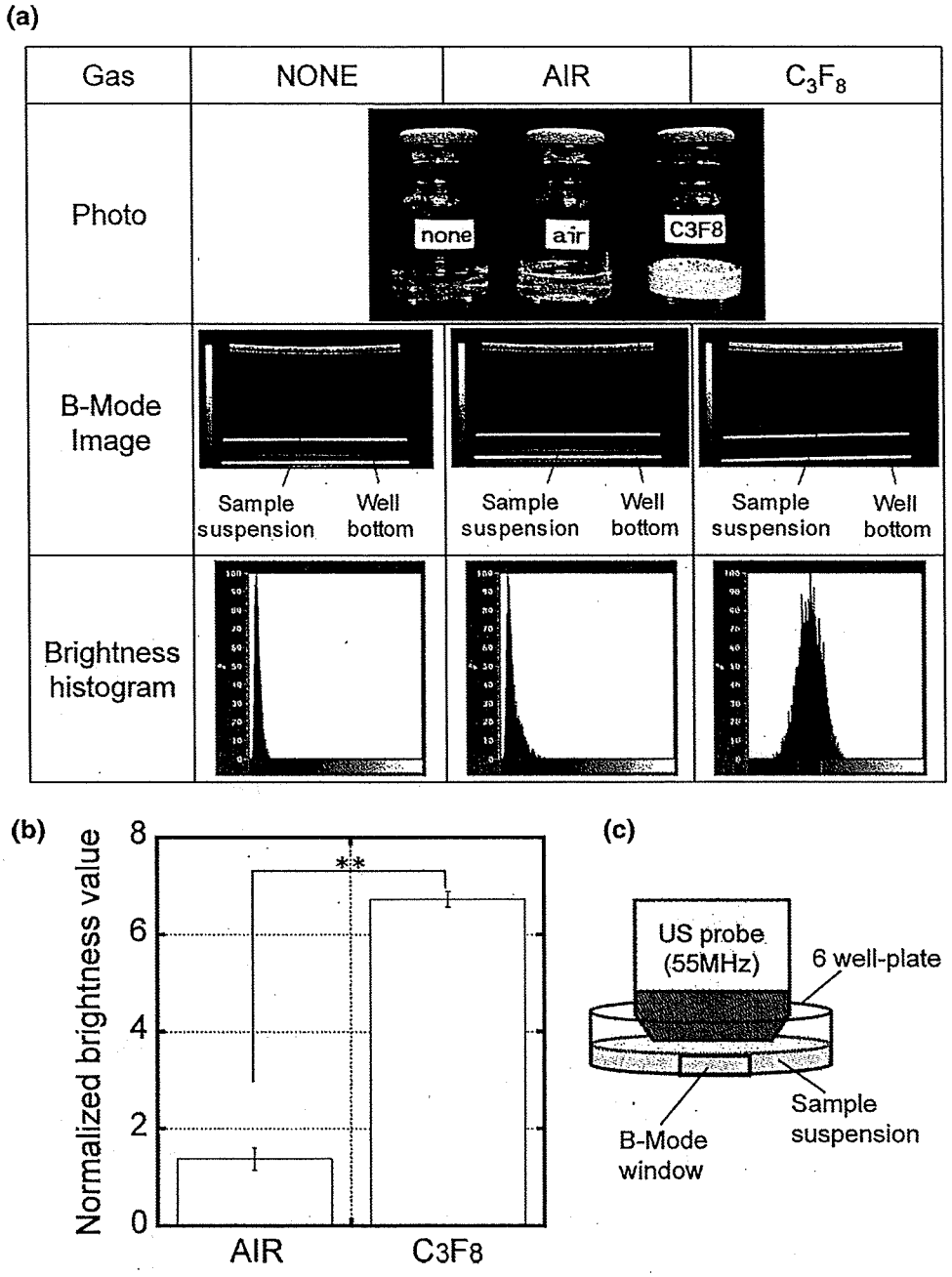

Fig. 2. Confirmation of gas entrapment into liposome. Photos, US B-mode images and brightness histograms of original liposome suspension (none), liposome sonicated under either atmospheric air (air) or C_3F_8 gas (C_3F_8) indicate encapsulation of gas under the presence of the C_3F_8 gas but not in the presence of air (a). The US B-mode images were captured as shown in the scheme for ultrasound imaging (c). There was a highly significant difference in brightness value between liposome sonicated under atmospheric air and C_3F_8 gas. The values were normalized with that of liposome without gas. $n = 4$, mean ± S.E. $^{**}P < 0.01$.

distribution of LSs, indicating that C_3F_8 gas bubbles are actually present inside some of the ALs.

Figure 6 shows a magnified image of the AL, stained at 80°C with the negative staining. The fluidity of lipid layers increases due to heat, and results in the enhanced penetration of the staining solution. The shell thickness was 5.6 nm, which accords with a biomembrane with a thickness of 7–10 nm. Thus, the AL shell is assumed to be a single lipid bilayer.

In order to investigate the AL structure in detail, we observed its cross-section, obtained from the double staining (Fig. 7). The black arrows in Fig. 7a indicate the presence of gas, while the white arrow indicates the presence of liquid. The percentage of

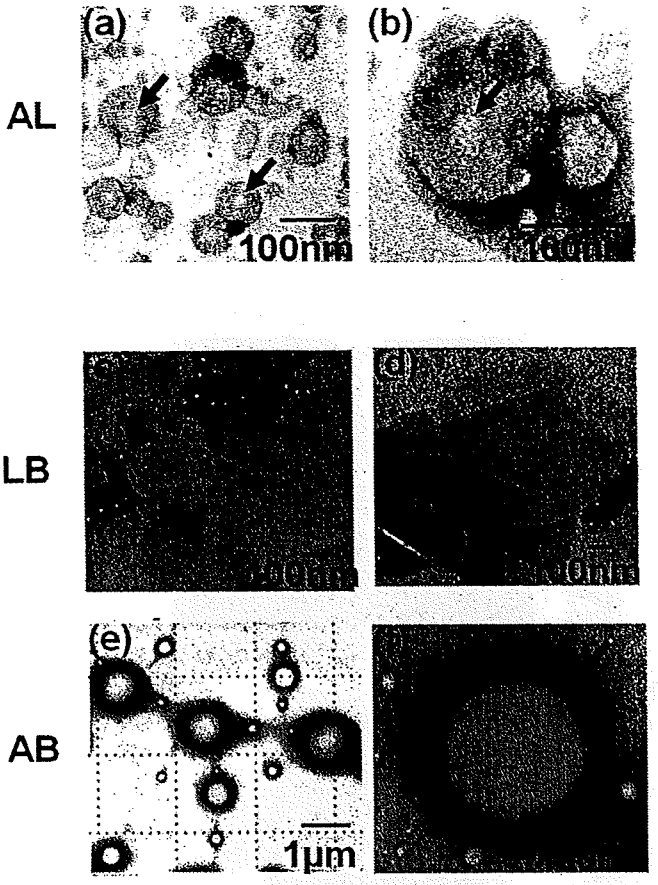

Fig. 3. Three types of ultrasound contrast agent from negative staining. AL: (a) ×50 000, (b) ×100 000. LB: (c) ×15 000, (d) ×10 000. AB: (e) ×3500, (f) ×20 000. The black arrows in (a) and (b) show where electron density was relatively low, indicating the presence of gas. The black arrow in (f) indicates albumin in filament form. (a)–(f) were stained at room temperature. (a), (b) JEOL JEM2000EX operated at 100 kV. (c)–(f) H-7600 operated at 80 kV.

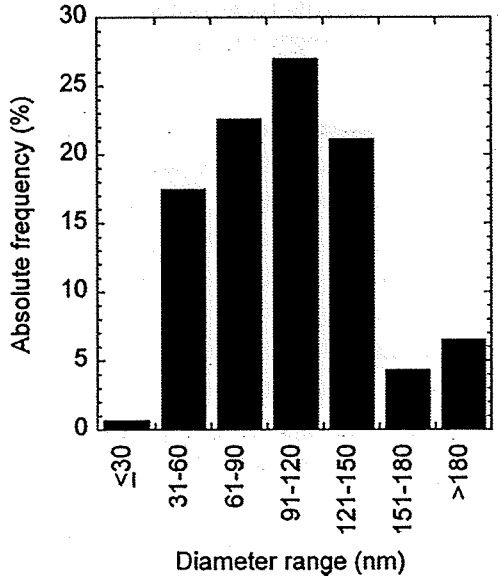

Fig. 4. Histogram of the absolute frequency distribution. The data were obtained from 10 TEM images. The maximum value was obtained within the class interval of 91–120 nm.

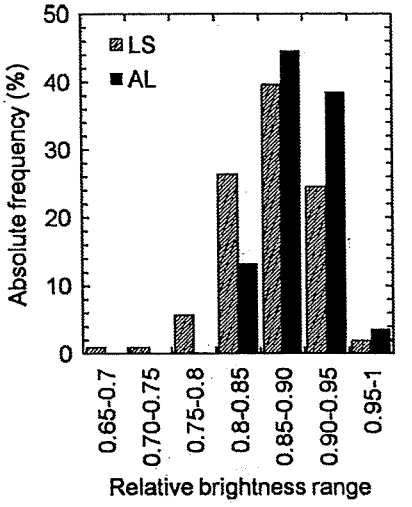

Fig. 5. Relative brightness range. AL and LS TEM micrographs were analyzed to assess the average brightness value of the inside of each kind of liposome. The inner area of each liposome image was digitally selected to measure its mean brightness value. Relative brightness values (measured mean brightness/background brightness) were obtained for 106 LSs and 83 ALs. The statistical distribution of ALs is slightly shifted to relative brightness values closer to 1 compared to the distribution of LSs, indicating that gas bubbles are actually present inside some of the ALs.

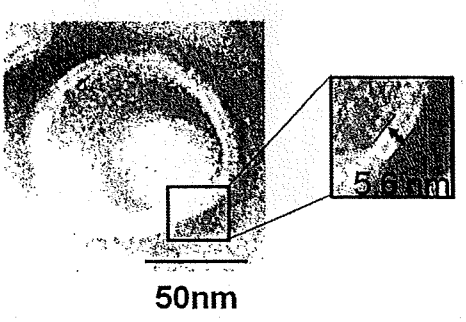

Fig. 6. Shell structure of AL. TEM micrograph of AL, negatively stained at 80°C. The distance between two lines in the magnified figure was 5.6 nm, indicating a single lipid bilayer. Original magnification, ×50 000. JEOL JEM2000EX operated at 100 kV.

AL was 24% (17 out of 70 liposomes). This value was similar to the 20% obtained and illustrated in Fig. 3a and b. Figure 7b shows that some ALs have an equal volume occupied by liquid and gas. The white arrows indicate the outside boundary, while the black arrows indicate the inside boundary. G shows the presence of gas, and L the presence of liquid. It is hard to judge whether the interface between the gas and the liquid within the AL is a gas/liquid interface or a lipid interface. Figure 7c shows an AL primarily occupied by gas. The proportion of gas relative to liquid is likely to vary depending on how the cross-section is cut. Figure 7d shows a liposome which was not sonicated, with a liquid-filled inside.

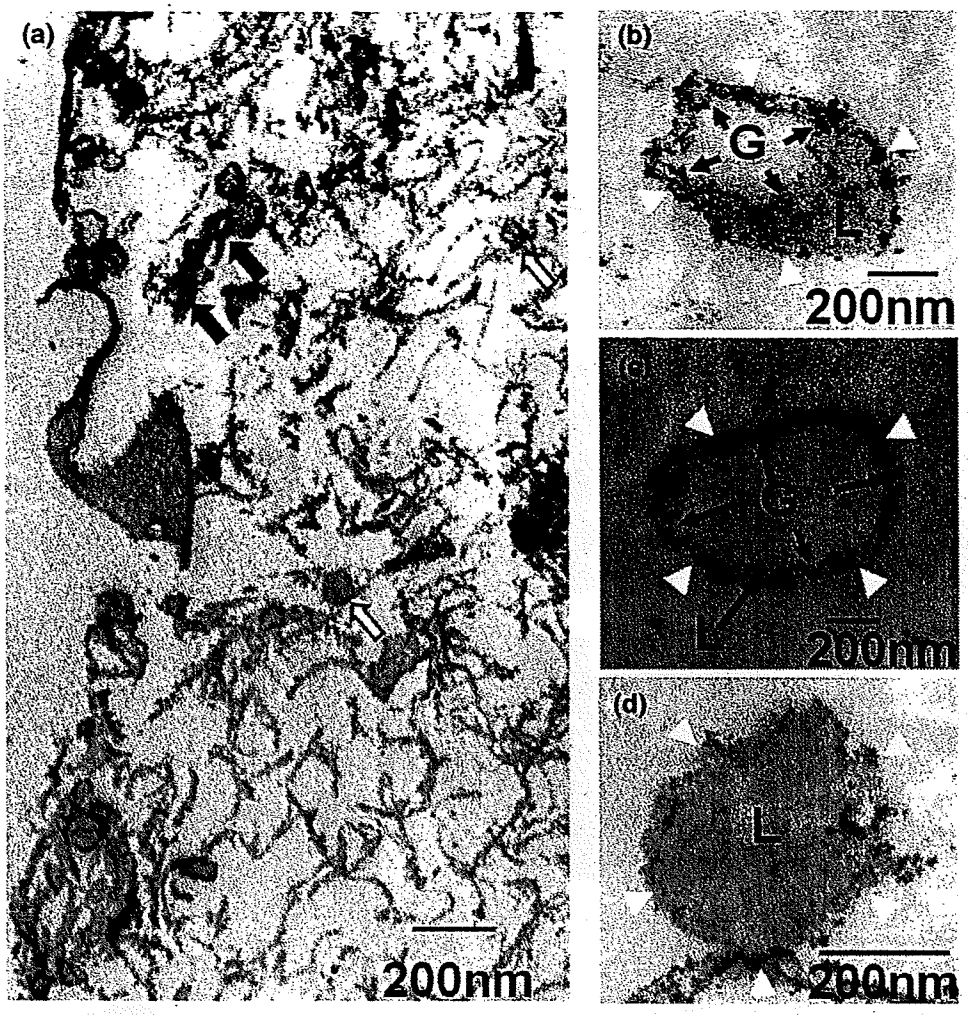

Fig. 7. Structure of AL from double staining. (a) The black arrows indicate the presence of gas in AL, while the white arrow indicates liquid. Original magnification: ×20 000. (b) AL occupied by ~50% (v/v) gas (G) and 50% (v/v) liquid (L). The white arrows indicate the outside boundary, while the black arrows indicate the inside boundary. Original magnification: ×30 000. (c) AL occupied mainly by gas (G). The liquid (L) portion was small. The white arrow indicates the outside boundary, while the black arrow indicates the inside boundary. Original magnification: ×20 000. (d) Liposome, which was not sonicated. The inside was filled with liquid (L). The white arrows indicate the outside boundary. Original magnification: ×50 000. (a)–(d) were obtained with JEOL JEM2000EX operated at 100 kV.

Discussion

The structure of an AL was investigated using TEM, and was compared with that for LB and AB. First we measured the diameter of AL by dynamic light scattering. The diameter of AL was ~200 nm (Table 1), which was about double the diameter calculated from the analysis of 10 TEM micrographs (Fig. 4). With dynamic light scattering, the size was measured immediately after AL production. TEM measurement indicated that the size of AL may have been influenced by the staining process and repeated electron beam exposure. These external factors might shift the frequency distribution to the lower value.

The zeta potential was derived from the hypothesis that ALs, LBs and ABs are hard particles [15]. ALs and LBs were found to be almost neutral, whereas AB had strong negative values (Table 1). As can be seen in TEM images (Fig. 3e and f), the electron beams were strongly scattered around the shell surface of the ABs. The key component of AB, albumin, was detected in its filament form. Ohshima [15] reported that the Smoluchowski equation cannot be applied to soft particles such as red blood cells, i.e. particles with an electric surface charge boundary in which a slip line exists. ABs are most likely to be a type of soft particle, for which this equation cannot be applied. Equations taking into account the properties of this kind of particles should be investigated.

From negative staining observations, it was assumed that AL have a single lipid bilayer as a shell structure (Fig. 6). The percentage of AL in which the presence of gas was detected was ~20%, and the proportion of volume occupied by gas and liquid varied depending on how the cross-sections were cut. Although it was hard to quantify the percentage of gas occupying the interior of AL due to the limited number of TEM images, it was clear from echogenicity that the C_3F_8 gas was actually encapsulated in ALs (Figs. 2 and 5).

Several acoustic liposome structures have been suggested [17,18]. Huang *et al.* [17] proposed that the internal volume was occupied by air and liquid compartments, and that the interface between the air and liquid compartments was a lipid monolayer. Suzuki *et al.* [18] suggested that both liquid and unilamellar lipids containing air were encapsulated by a single lipid bilayer. In the present study, we observed that gas and liquid seemed to be encapsulated together by a single lipid bilayer. However, we could not judge whether the interface between the gas and the liquid was the gas/liquid interface or the lipid interface.

The co-existence of gas and liquid in ALs provides evidence of its echogenicity and drug-carrying capabilities. Further, the tissue specificity of ALs can be improved by conjugating ligands against the target tissue with PEG on the AL surface. Recently, a high-frequency ultrasound system with ALs has been developed and applied so far to the imaging of anterior segment of the eye [19], skin [20] and tumor vasculature [21]. Studies have shown that the permeability of the tumor vasculature is enhanced, and the phenomenon is recognized as the EPR effect [11].

Most anticancer drugs have diameters of 10–120 nm: Genexol-PM (20–50 nm in diameter), Doxil (80–90 nm in diameter), Abraxane (120 nm in diameter) [12]. Sonoporation delivery efficiency, *in vivo* behavior and tissue-specificity of ALs would possibly be enhanced if the diameter was controlled within the range of 10–120 nm, the surface was positively or negatively charged, and ligands against the tumor were conjugated to PEG on the surface [22–24].

Concluding remarks

In summary, the findings of the present study indicate that AL have a shell consisting of a single lipid bilayer and can encapsulate both drugs and gas. The PEG distributed over the surface can be conjugated with tissue-specific ligands. Developing functional AL will assure the effectiveness of sonoporation.

Funding

This work was supported by a Grant-in-Aid for Scientific Research (B) [20300173 to T.K., 19390507 to S.M.]; a Grant-in-Aid for Scientific Research on Priority Area, MEXT [20015005 to T.K.]; a Grant for Research on Advanced Medical Technology, the Ministry of Health, Labor and Welfare of Japan [H19-nano-010 to T.K.]; a Grant for Research on Development of Systems and Technology for Advanced Measurement and Analysis, JST [T.K.]; and a Grant-in-Aid for JSPS Fellows [21-7271 to S.H.].

Acknowledgements

The authors would like to thank Yukiko Watanabe, Rui Chen and Li Li, for their technical assistance.

References

1 Kodama T, Tomita Y, Koshiyama K, and Blomley M J (2006) Transfection effect of microbubbles on cells in superposed ultrasound waves and behavior of cavitation bubble. *Ultrasound Med. Biol.* **32**: 905–914.

2 Lindner J R (2004) Microbubbles in medical imaging: current applications and future directions. *Nat. Rev. Drug Discov.* **3**: 527–532.

3 Shohet R V, Chen S, Zhou Y T, Wang Z, Meidell R S, Unger R H, and Grayburn P A (2000) Echocardiographic destruction of albumin microbubbles directs gene delivery to the myocardium. *Circulation* **101**: 2554–2556.

4 Christiansen J P, French B A, Klibanov A L, Kaul S, and Lindner J R (2003) Targeted tissue transfection with ultrasound destruction of plasmid-bearing cationic microbubbles. *Ultrasound Med. Biol.* **29**: 1759–1767.

5 Suzuki R, Takizawa T, Negishi Y, Utoguchi N, Sawamura K, Tanaka K, Namai E, Oda Y, Matsumura Y, and Maruyama K (2008) Tumor specific ultrasound enhanced gene transfer *in vivo* with novel liposomal bubbles. *J. Control. Release* **125**: 137–144.

6 Suzuki R, Oda Y, Utoguchi N, Namai E, Taira Y, Okada N, Kadowaki N, Kodama T, Tachibana K, and Maruyama K (2009) A novel strategy utilizing ultrasound for antigen delivery in dendritic cell-based cancer immunotherapy. *J. Control. Release* **133**: 198–205.

7 Church C C (1995) The effrcts of an elastic solid-surface layer on the radial pulsations of gas-bubbles. *J. Acoust. Soc. Am.* **97**: 1510–1521.

8 Kodama T, Tomita Y, Watanabe Y, Koshiyama K, Yano T, and Fujikawa S (2009) Cavitation bubbles mediated molecular delivery during sonoporation. *J. Biomech. Sci. Eng.* **4**: 124–140.

9 Suzuki R, Takizawa T, Negishi Y, Hagisawa K, Tanaka K, Sawamura K, Utoguchi N, Nishioka T, and Maruyama K (2007) Gene delivery by combination of novel liposomal bubbles with perfluoropropane and ultrasound. *J. Control. Release* **117**: 130–136.

10 Klibanov A L, Maruyama K, Torchilin V P, and Huang L (1990) Amphipathic polyethyleneglycols effectively prolong the circulation time of liposomes. *FEBS Lett.* **268**: 235–237.

11 Matsumura Y and Maeda H (1986) A new concept for macromolecular therapeutics in cancer chemotherapy: mechanism of tumoritropic

accumulation of proteins and the antitumor agent smancs. *Cancer Res.* **46**: 6387–6392.

12 Davis M E, Chen Z G, and Shin D M (2008) Nanoparticle therapeutics: an emerging treatment modality for cancer. *Nat. Rev. Drug Discov.* **7**: 771–782.

13 Aoi A, Watanabe Y, Mori S, Takahashi M, Vassaux G, and Kodama T (2008) Herpes simplex virus thymidine kinase-mediated suicide gene therapy using nano/microbubbles and ultrasound. *Ultrasound Med. Biol.* **34**: 425–434.

14 Watanabe Y, Aoi A, Horie S, Tomita N, Mori S, Morikawa H, Matsumura Y, Vassaux G, and Kodama T (2008) Low-intensity ultrasound and microbubbles enhance the antitumor effect of cisplatin. *Cancer Sci.* **99**: 2525–2531.

15 Ohshima H (1994) Electrophoretic mobility of soft particles. *J. Colloid Interface Sci.* **163**: 474–483.

16 Yanai H (2007) *Statcel—The Useful Add-in Forms on Excel.* (OMS, Tokyo).

17 Huang S L, and Macdonald R C (2004) Acoustically active liposomes for drug encapsulation and ultrasound-triggered release. *Biochim. Biophys. Acta* **1665**: 134–141.

18 Suzuki R, Takizawa T, Negishi Y, Utoguchi N, and Maruyama K (2008) Effective gene delivery with novel liposomal bubbles and ultrasonic destruction technology. *Int. J. Pharm.* **354**: 49–55.

19 Pavlin C J, and Foster F S (1998) Ultrasound biomicroscopy. High-frequency ultrasound imaging of the eye at microscopic resolution. *Radiol. Clin. North Am.* **36**: 1047–1058.

20 Vogt M, and Ermert H (2008) Limited-angle spatial compound imaging of skin with high-frequency ultrasound (20 MHz). *IEEE Trans. Ultrason. Ferroelectr. Freq Control* **55**: 1975–1983.

21 Lyshchik A, Fleischer A C, Huamani J, Hallahan D E, Brissova M, and Gore J C (2007) Molecular imaging of vascular endothelial growth factor receptor 2 expression using targeted contrast-enhanced high-frequency ultrasonography. *J. Ultrasound Med.* **26**, 1575–1586.

22 Schneider M (2008) Molecular imaging and ultrasound-assisted drug delivery. *J. Endourol.* **22**: 795–802.

23 Kaufmann B A, and Lindner J R (2007) Molecular imaging with targeted contrast ultrasound. *Curr. Opin. Biotechnol.* **18**: 11–16.

24 Palmowski M, Huppert J, Hauff P, Reinhardt M, Schreiner K, Socher M A, Hallscheidt P, Kauffmann G W, Semmler W, and Kiessling F (2008) Vessel fractions in tumor xenografts depicted by flow- or contrast-sensitive three-dimensional high-frequency Doppler ultrasound respond differently to antiangiogenic treatment. *Cancer Res.* **68**: 7042–7049.

Journal of Controlled Release 133 (2009) 198–205

Contents lists available at ScienceDirect

Journal of Controlled Release

journal homepage: www.elsevier.com/locate/jconrel

A novel strategy utilizing ultrasound for antigen delivery in dendritic cell-based cancer immunotherapy

Ryo Suzuki [a], Yusuke Oda [a], Naoki Utoguchi [a], Eisuke Namai [a], Yuichiro Taira [a], Naoki Okada [b], Norimitsu Kadowaki [c], Tetsuya Kodama [d], Katsuro Tachibana [e], Kazuo Maruyama [a,*]

[a] Department of Biopharmaceutics, School of Pharmaceutical Sciences, Teikyo University, 1091-1 Suwarashi, Sagamiko-cho, Sagamihara, Kanagawa 229-0195, Japan
[b] Department of Biotechnology and Therapeutics, Graduate School of Pharmaceutical Sciences, Osaka University, 1-6 Yamadaoka, Suita, Osaka 565-0871, Japan
[c] Department of Hematology and Oncology, Graduate School of Medicine, Kyoto University, 54 Shogoin Kawara-cho, Sakyo-ku, Kyoto 606-8507, Japan
[d] Department of Biomedical Engineering, Graduate School of Biomedical Engineering, Tohoku University, 2-1 Seiryo-machi, Aoba-ku, Sendai 980-8575, Japan
[e] Department of anatomy, School of medicine, Fukuoka University, 7-45-1 Nanakuma, Jonan-ku, Fukuoka 814-0180, Japan

ARTICLE INFO

Article history:
Received 12 August 2008
Accepted 16 October 2008
Available online 31 October 2008

Keywords:
Dendritic cells
Antigen delivery system
Cancer immunotherapy
Ultrasound
Liposomes

ABSTRACT

In dendritic cell (DC)-based cancer immunotherapy, it is important that DCs present peptides derived from tumor-associated antigens on MHC class I, and activate tumor-specific cytotoxic T lymphocytes (CTLs). However, MHC class I generally present endogenous antigens expressed in the cytosol. We therefore developed an innovative approach capable of directly delivering exogenous antigens into the cytosol of DCs; i.e., a MHC class I-presenting pathway. In this study, we investigated the effect of antigen delivery using perfluoropropane gas-entrapping liposomes (Bubble liposomes, BLs) and ultrasound (US) exposure on MHC class I presentation levels in DCs, as well as the feasibility of using this antigen delivery system in DC-based cancer immunotherapy. DCs were treated with ovalbumin (OVA) as a model antigen, BLs and US exposure. OVA was directly delivered into the cytosol but not via the endocytosis pathway, and OVA-derived peptides were presented on MHC class I. This result indicates that exogenous antigens can be recognized as endogenous antigens when delivered into the cytosol. Immunization with DCs treated with OVA, BLs and US exposure efficiently induced OVA-specific CTLs and resulted in the complete rejection of E.G7-OVA tumors. These data indicate that the combination of BLs and US exposure is a promising antigen delivery system in DC-based cancer immunotherapy.

1. Introduction

Dendritic cells (DCs), which are unique antigen-presenting cells capable of priming naive T cells, are promising vaccine carriers for cancer immunotherapy [1]. To induce efficiently a tumor-specific cytotoxic T-lymphocyte (CTL) response, DCs should abundantly present epitope peptides derived from tumor-associated antigens (TAAs) via major histocompatibility complex (MHC) class I molecules [2]. In general, the majority of peptides presented via the MHC class I molecules are generated from endogenously synthesized proteins that are degraded by the proteasome [3]. On the other hand, exogenous antigens such as TAAs for DCs are preferentially presented on MHC class II molecules [3]. In order to prime efficiently TAAs specific for CTLs, it is important to develop a novel antigen delivery system, which can induce MHC class I restricted TAA presentation on DCs. Several researchers are developing antigen delivery tools based on the cross presentation theory of exogenous antigens for DCs [4–8]. In these studies, various types of antigen delivery carriers such as liposomes [6,7], poly(γ-glutamic acid) nanoparticles [5] and cholesterol pullulan nanoparticles [8], all of which can deliver antigen into DCs via the endocytosis pathway, have been developed. We have reported that IgG modified liposomes with entrapped antigen can induce cross presentation of exogenous antigen for DCs on MHC class I molecules [9]. These carriers deliver antigens into DCs via an endocytosis mechanism, with delivery thought to be due to exogenous antigen leaking from the endosome into the cytosol. It is therefore important to design an antigen delivery system which does not rely on the endocytosis pathway. In other study, it was reported that DCs pulsed with exogenous antigens by electroporation presented their antigens on MHC class I molecules and resulted

Abbreviations: Alexa-OVA, Alexa Fluor 488-conjugated ovalbumin; BL, Bubble liposome; CTL, cytotoxic T lymphocyte; DC, dendritic cell; DSPC, 1,2-distearoyl-sn-glycero-phosphatidylcholine; DSPE-PEG(2k)-OMe, 1,2-distearoyl-sn-glycero-3-phosphatidyl-ethanolamine-methoxypolyethyleneglycol; ER, endoplasmic reticulum; FBS, fetal bovine albumin; HLA, human leukocyte antigen; MHC, major histocompatibility complex; MTT, 3-(4,5-s-dimethylthiazol-2-yl)-2,5-diphenyl tetrazolium bromide; NaN_3, sodium azide; OVA, ovalbumin; PBS, phosphate buffer saline; US, ultrasound; TAA, tumor associated antigen.

* Corresponding author. Department of Biopharmaceutics, School of Pharmaceutical Sciences, Teikyo University, 1091-1 Suwarashi, Sagamiko-cho, Sagamihara, Kanagawa 229-0195, Japan. Tel.: +81 42 685 3722; fax: +81 42 685 3432.
E-mail address: maruyama@pharm.teikyo-u.ac.jp (K. Maruyama).

0168-3659/$ – see front matter © 2008 Elsevier B.V. All rights reserved.
doi:10.1016/j.jconrel.2008.10.015

in inducing MHC class I-mediated antitumor immunity. Although electroporation is commonly utilized as gene delivery method and deliver gene such as DNA and RNA into cytosol, Kim K.W. et al and Weiss J.M. et al. apply this system to antigen delivery into DCs [10,11]. Their reports also demonstrate the importance of delivering exogenous antigens into cytosol of DCs to induce MHC class I presentation of the antigens.

It has been reported that ultrasound (US) increases the permeability of the plasma membrane, which encourages the entry of DNA into cells [12,13]. The first studies applying US for gene delivery used frequencies in the range of 20–50 kHz [12,14]. However, these frequencies, along with cavitation, are also known to induce tissue damage if not properly controlled [15–17]. To address this problem, many studies into using therapeutic US for gene delivery have used frequencies of 1–3 MHz, intensities of 0.5–2.5 W/cm^2 and a pulse-mode [18–20]. In addition, it was reported that the combination of therapeutic US and microbubble echo contrast agents could enhance gene transfection efficiency [21–27]. In this method, DNA is effectively and directly transferred into the cytosol. This system has been applied to deliver proteins into cells [28,29], but not yet to deliver antigens into DCs for the purpose of cancer immunotherapy. Previously, we developed novel liposomal bubbles containing nanobubbles of the US imaging gas, perfluoropropane [30–34] and suggested that these "Bubble liposomes" (BLs) might be used as novel non-viral gene delivery tools if combined with US exposure. In the case of DCs, the antigen delivered into the cytosol would present on MHC class I molecules and result in priming antigen-specific CTLs. In this study, we examined the effectiveness of BLs combined with US exposure to deliver antigen into DCs. In addition, the effectiveness of this antigen delivery system in DC-based cancer immunotherapy was assessed.

2. Materials and methods

2.1. Cells

T cell hybridoma CD8-OVA1.3 (a kind gift from Dr. C.V. Harding, Department of Pathology, Case Western Reserve University, Cleveland, OH, USA), a cell type that recognizes SIINFEKL:H-2K^b complexes [35], was cultured in Dulbecco's modified Eagle's medium (DMEM, Sigma Chemical Co., St. Louis, MO, USA) supplemented with 10% heat inactivated fetal bovine serum (FBS, GIBCO, Invitrogen Co., Carlsbad, CA, USA), 50 μM 2-mercaptethanol (2-ME), 250 μg/ml amphotericin B (Wako Pure Chemical Industries, Ltd., Osaka, Japan) and 50 μg/ml gentamycin (Wako Pure Chemical Industries). EL-4 murine thymoma cells were cultured in RPMI 1640 supplemented with 10% FBS and 50 μM 2-ME. E.G7-OVA cells (OVA cDNA transfectant of EL4 cells) were maintained in RPMI 1640 supplemented with 10% FBS, 50 μM 2-ME and 400 μg/ml GENETICIN (G418 sulfate, GIBCO, Invitrogen). All culture media contained 50 U/ml penicillin and 50 μg/ml streptomycin (Wako Pure Chemical Industries).

2.2. Generation of mouse bone marrow-derived DCs

DCs were generated from bone marrow cells as described elsewhere [36]. Briefly, bone marrow cells were isolated from C57BL/6 mice and were cultured in RPMI 1640 with 10% FBS, 50 U/ml penicillin, 50 μg/ml streptomycin and 40 ng/ml mouse granulocyte-macrophage colony-stimulating factor (GM-CSF). After 8–16 days of culture, non-adherent cells were collected and used as DCs.

2.3. Preparation of BLs

Liposomes composed of 1,2-distearoyl-sn-glycero-phosphatidylcholine (DSPC) (NOF Corp., Tokyo, Japan) and 1,2-distearoyl-sn-glycero-3-phosphatidyl-ethanolamine-methoxypolyethyleneglycol (DSPE-PEG(2k)-OMe, (PEG Mw=ca. 2000), NOF) (94 : 6 (m/m)) were prepared by reverse phase evaporation. Briefly, all reagents (total lipid: 100 μmol) were dissolved in 8 ml of 1:1 (v/v) chloroform/diisopropyl ether, then 4 ml of phosphate buffered saline (PBS) was added. The mixture was sonicated and evaporated at 65 °C. The solvent was completely removed, and the size of the liposomes was adjusted to less than 200 nm using an extruding apparatus (Northern Lipids Inc., Vancouver, BC, Canada) and sizing filters (pore sizes: 100 and 200 nm; Nuclepore Track-Etch Membrane, Whatman plc, UK). After sizing, the liposomes were sterilized by passing them through a 0.45 μm pore size filter (MILLEX HV filter unit, Durapore PVDF membrane, Millipore Corp., MA, USA). The size of the liposomes was measured by dynamic light scattering (ELS-800, Otsuka Electronics Co., Ltd., Osaka, Japan). The average diameter of these liposomes was between 150–200 nm. Lipid concentration was measured using the Phospholipid C test (Wako Pure Chemical Industries). BLs were prepared from the liposomes and perfluoropropane gas (Takachiho Chemical Industrial Co., Ltd., Tokyo, Japan) [31,33]. Briefly, 5 ml sterilized vials containing 2 ml of the liposome suspension (lipid concentration: 2 mg/ml) were filled with perfluoropropane, capped, and then supercharged with 7.5 ml of perfluoropropane. The vial was placed in a bath-type sonicator (42 kHz, 100 W; BRANSONIC 2510J-DTH, Branson Ultrasonics Co., Danbury, CT, USA) for 5 min to form the BLs. In this method, the liposomes were reconstituted by sonication under the condition of supercharge with perfluoropropane in the 5 mL vial container. At the same time, perfluoropropane would be entrapped within lipids like micelles, which were made by DSPC and DSPE-PEG(2k)-OMe from liposome composition, to form nanobubbles. The lipid nanobubbles were encapsulated within the reconstituted liposomes, which sizes were changed into around 1 μm from 150–200 nm of original.

2.4. Antigen trafficking into DCs after antigen delivery with BLs and US exposure

Alexa Fluor 488 conjugated OVA (Alexa-OVA) was prepared with Alexa Fluor 488 succinimidyl ester (Molecular Probes, Invitrogen) according to the instruction manual. DCs (1×10^5 cells/ml) were cultured in a glass bottom dish (IWAKI, Asahi Glass Co. Ltd., Tokyo, Japan) overnight. After washing the cells with OptiMEM (Invitrogen), BLs (240 μg/ml) and Alexa-OVA (50 μg/ml) were added to the dish. Then, the DCs were exposed to US exposure (frequency: 2 MHz, duty: 10%, burst rate: 2.0 Hz, intensity 2.0 W/cm^2, time: 3×10 s (interval: 10 s)) using a Sonopore 4000 (6 mm diameter probe; Nepa Gene Co. Ltd., Chiba, Japan). This condition was decided referring to our reports about gene delivery [31,33] and Guo et al.'s report about the repeat US exposure with interval [37], and from the viewpoint of cytotoxicity for DCs. After US exposure, the DCs were incubated for 1 h at 37 °C, then washed with PBS, fixed with 3% paraformaldehyde for 10 min, and treated with 0.1% Triton X-100 (Wako Pure Chemical Industries) for 5 min. In addition, some DCs were washed with PBS, their nuclei were stained with propidium iodide (0.5 μg/ml) (Wako Pure Chemical Industries), and antigen trafficking was observed with a confocal laser microscope.

2.5. Antigen delivery following inhibition of the endocytosis pathway in DCs

DCs were pretreated with OptiMEM containing 10 mM NaN_3 for 1 h at 4 °C to inhibit the endocytosis pathway. After washing the cells, BLs (240 μg/ml) and Alexa-OVA (50 μg/ml) were added to the DCs in OptiMEM containing 10 mM sodium azide (NaN_3). The DCs were exposed to US exposure (frequency: 2 MHz, duty: 10%, burst rate: 2.0 Hz, intensity 2.0 W/cm^2, time: 3×10 s (interval: 10 s)), then washed with PBS containing10 mM NaN_3. After US exposure, DCs were fixed and their nuclei were stained as described above (2.4.).

2.6. Flow cytometry analysis of antigen delivery into DCs with BLs and US exposure

Alexa-OVA was delivered into DCs under inhibited endocytosis conditions as described above (2.5.). After washing, the DCs were stained with propidium iodide (100 ng/ml) and analyzed by flow cytometry (FACSCalibur, Becton, Dickinson and Company, Franklin Lakes, NJ, USA). In this study, living DCs (1×10^4 cells) were analyzed by gating out propidium iodide staining cells.

2.7. Assessment of MHC class I restricted OVA presentation

DCs (2.5×10^5 cells/500 μl/well (48-well plate)) were pulsed with OVA alone (0, 10, 100, 1000 μg/ml) or OVA (0, 10, 100, 1000 μg/ml) using US exposure (frequency: 2 MHz, duty: 10%, burst rate: 2.0 Hz, intensity 2.0 W/cm^2, Time: 3×10 s (interval: 10 s)) and/or BLs (240 μg/ml). After US exposure, the DCs were incubated for 1 h at 37 °C, then washed with PBS. After culturing for 24 h, the DCs were co-cultured for 20 h with T cell hybridoma CD8-OVA1.3 (2×10^5 cells/well) that recognizes SIINFEKL: H-2K^b complexes. The concentration of IL-2 in the supernatants was measured using an IL-2 ELISA Kit (BioSource International, Inc., Camarillo, CA, USA).

2.8. Assessment of cytotoxicity to DCs by the treatment of BLs and US exposure

DCs (2.5×10^5 cells/500 μl/well (48-well plate)) were treated with BLs (240 μg/ml) and/or US exposure (frequency: 2 MHz, duty: 10%, burst rate: 2.0 Hz, intensity 2.0 W/cm^2, Time: 3×10 s (interval: 10 s)). After US exposure, DCs were incubated for 1 h at 37 °C, and washed with PBS. The DCs were resuspended with cuture medium (250 μl) and cultured for 48 h. Cell viability was assayed using MTT (3-(4,5-s-dimethylthiazol-2-yl)-2,5-diphenyl tetrazolium bromide, Dojindo, Kumamoto, Japan) as described by Mosmann with minor modifications [38]. Briefly, MTT (5 mg/mL, 25 μL) was added to each well and the cells were incubated at 37 °C for 4 h. The formazan product was dissolved in 250 μL of 10% sodium dodecyl sulfate (SDS, Wako Pure Chemical Ind. Co., Ltd. Osaka, Japan) containing 15 mM HCl. Color intensity was measured using a microplate reader (POWERSCAN HT; Dainippon Pharmaceutical, Osaka, Japan) at test and reference wavelengths of 595 and 655 nm, respectively.

2.9. Immunization of mice with DCs and cytotoxicity assay

DCs (2.5×10^5 cells/500 μl/well) were pulsed with OVA alone (100 μg/ml) or OVA (100 μg/ml) using US exposure (frequency: 2 MHz, duty: 10%, burst rate: 2.0 Hz, intensity 2.0 W/cm^2, Time: 3×10 s (interval: 10 s)) and/or BLs (240 μg/ml) on a 48-well plate, then collected from 10 wells and seeded into 6-well plates. After 1 h incubation at 37 °C, the DCs were washed and cultured for 24 h at 37 °C. After washing, DCs (1×10^6 cells/100 μl) were intradermally injected into the backs of C57BL/6 mice. After 7 days, the mice were re-immunized. Seven days after the second immunization, splenocytes were obtained from five mice, and the splenocytes were pooled and stimulated with mitomycin C-treated E.G7-OVA cells at a ratio of 10:1 for 5 days. The stimulated splenocytes were used as effector cells for the cytotoxicity assay, using EL-4 or E.G7-OVA as the target cells in a flow cytometric assay employing two fluorochromes [39]. PKH-67, a fluorochrome which fluoresces green, binds to the cytoplasmic membrane and does not leak or transfer, was used to identify the target cell population. Propidium iodide fluoresces red and was used to detect non-viable cells. Use of these two fluorochromes and two parameter analyses allowed the identification of four subpopulations in the sample: live effectors, dead effectors, live targets and dead targets. By enumerating these subpopulations, the percent target lysis can be calculated.

2.10. Antitumor effect by prior immunization with antigen-pulsed DCs

DCs (2.5×10^5 cells/500 μl/well) were pulsed with OVA alone (100 μg/ml) or OVA (100 μg/ml) using US exposure (frequency: 2 MHz, duty: 10%, burst rate: 2.0 Hz, intensity 2.0 W/cm^2, Time: 3×10 s (interval: 10 s)) and/or BLs (240 μg/ml) on a 48-well plate, then collected from 10 wells and seeded into 6-well plates. After 1 h incubation at 37 °C, the DCs were washed and cultured for 24 h at 37 °C. After washing, the DCs (1×10^6 cells/100 μl) were intradermally immunized into the backs of C57BL/6 mice twice at intervals of one week. Seven days after the second immunization, E.G7-OVA cells (1×10^6 cells) were intradermally inoculated into the backs of mice and the size of the tumors was monitored using the formula: (major axis×minor axis^2)×0.5. All treated groups contained five mice.

2.11. Re-challenge of tumor cells

E.G7-OVA cells (1×10^6 cells) were injected into mice that were resistant to tumor cells due to immunization with DCs treated with BLs, US exposure and OVA. Untreated mice were used as controls to confirm the development of cancer following the first inoculation with E.G7-OVA cells. All treated groups contained five mice.

2.12. Treatment of tumor-bearing mice with antigen-pulsed DCs

E.G7-OVA cells (1×10^6 cells) were intradermally inoculated into the backs of C57BL/6 mice. On day 9, when the tumors were between 8–10 mm, OVA pulsed DCs (1×10^6 cells) prepared as described above were intradermally injected into the backs of the mice. On day 12, DCs were injected similarly. Tumor sizes were monitored from the day of inoculation. All treated groups contained five mice.

2.13. Statistical analysis

Differences in IL-2 secretion between the experimental groups were compared using non-repeated measures ANOVA and Dunnett's test.

3. Results

3.1. Antigen delivery by BLs and sonoporation into the cytosol of DCs lacking the endocytosis pathway

We examined antigen trafficking following delivery using a combination of BLs and US exposure (Fig. 1(a)). In DCs treated with Alexa-OVA in the presence or absence of either BLs or US exposure, the fluorescence from Alexa-OVA appeared as dots in the cytosol. On the other hand, in DCs treated with Alexa-OVA, BLs and US exposure, the fluorescence appeared as dots, but also as diffused fluorescence in the cytosol. To confirm this, antigen delivery was examined following inhibition of the endocytosis pathway in DCs by treatment with sodium azide (Fig. 1(b)). In DCs treated with Alexa-OVA either with or without BLs or US exposure, the fluorescence derived from Alexa-OVA was not observed. On the other hand, in DCs treated with Alexa-OVA, BLs and US exposure, fluorescence was observed in the cytosol even when the endocytosis pathway in DCs was inhibited. In addition, the efficiency of antigen delivery following inhibition of the endocytosis pathway was assessed using flow cytometory (Fig. 1(c)). The fluorescence intensity of DCs treated with Alexa-OVA, BLs and US exposure was higher than that of DCs treated with Alexa-OVA alone, or of Alexa-OVA and BLs or US exposure. These data support the data shown in Fig. 1(b), indicating that Alexa-OVA is observed in the cytosol when DCs are only treated with BLs and US exposure, even when the endocytosis pathway is

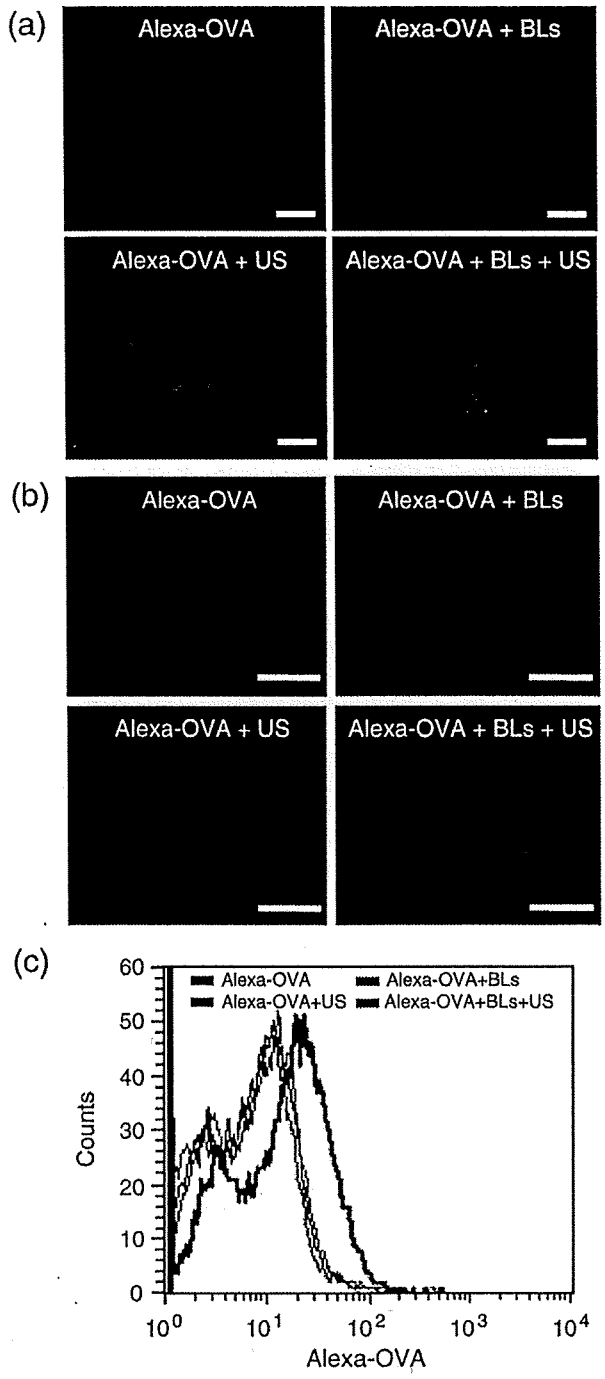

Fig. 1. Intracellular antigen delivery into DCs using BLs and US exposure. (a) Uptake of Alexa-OVA into DCs. DCs were cultured in a glass bottom dish overnight. After washing the cells, Alexa-OVA was added to the dish. Then, the DCs were exposed to US in the presence or absence of BLs and incubated for 1 h at 37 °C. The DCs were washed with PBS, fixed, and the nuclei were stained with propidium iodide. The uptake of Alexa-OVA was observed using a confocal laser microscope. (b) Intracellular delivery of Alexa-OVA into DCs using BLs and US. DCs were pretreated with OptiMEM containing 10 mM NaN_3 for 1 h at 4 °C to inhibit the endocytosis pathway. After washing the cells, Alexa-OVA was added to the DCs in OptiMEM containing10 mM NaN_3. Then, the DCs were exposed to US in the presence or absence of BLs. After US exposure, the DCs were washed with PBS containing 10 mM NaN_3, fixed, and the nuclei were stained with propidium iodide. Intracellular trafficking of Alexa-OVA in the DCs was observed using a confocal laser microscope. Scale bar shows 5 μm. (c) Flow cytometry analysis of DCs containing Alexa-OVA delivered using BLs and US. Alexa-OVA was delivered into the cell interior of the DCs during endocytosis inhibition. After washing the cells, the DCs were analyzed by flow cytometry.

inhibited. These results suggest that the combination of BLs and US exposure can be used to directly deliver antigens into the cytosol of DCs in the absence of endocytosis.

3.2. MHC class I presentation of exogenous antigen delivered into DCs by BLs and US exposure

Exogenous antigen delivered into the cytosol of DCs by BLs and US exposure is recognized as endogenous antigen by DCs and leads to the efficient presentation of peptides derived from exogenous antigens on MHC class I molecules. Thus, we examined whether antigen delivery by BLs and US exposure resulted in the efficient presentation of peptides on MHC class I molecules and the stimulation of $CD8^+$ T cells. C57BL/6-derived OVA-specific T cell hybridoma CD8-OVA1.3 was co-cultured with mouse bone marrow-derived DCs pulsed with antigen. As shown in Fig. 2, CD8-OVA1.3 cells stimulated with DCs pulsed with soluble OVA, either treated or untreated by BLs or US exposure did not secrete a significant amount of IL-2. Of note, a larger amount of IL-2 was secreted by CD8-OVA1.3 cells stimulated with DCs pulsed with OVA treated with a combination of BLs and US exposure. These data indicate that antigen delivery by BLs to DCs upon sonoporation results in the presentation of peptides derived from OVA on MHC class I molecules. In this data, the level of IL-2 secretion increased depending on OVA concentration and reached plateau in 100 μg/ml of OVA concentration. Therefore, we used this OVA concentration (100 μg/ml) in further examinations.

3.3. Cytotoxicity to DCs by the treatment of BLs and US exposure

In this antigen delivery system using BLs and US exposure, the transient pores would be provided on the membrane of DCs. Therefore, it is concerned that the DCs are injured by US exposure in the presence of BLs. To assess the cytotoxicity to DCs by the treatment of BLs and US exposure, we examined about the viability of DCs (Fig. 3). In the treatment of DC with BLs and/or US exposure, the viability of DCs treated with BLs, US exposure or BLs/US exposure was 83 ± 11%, 96 ± 5% or 87 ± 13%, respectively. This result shows that there is not serious damage to DCs even under the condition of inducing transient pores on the membrane of DCs treated with BLs and US exposure.

3.4. Induction of antigen-specific CTL response in the immunization of DCs pulsed with antigen using BLs and US exposure

To examine whether efficient peptide presentation on MHC class I molecules leads to strong induction of antigen-specific CTLs *in vivo*, we immunized C57BL/6 mice twice with bone marrow-derived DCs that had been treated with various antigen delivery techniques. Thereafter, splenocytes were isolated, and a cytotoxicity assay was

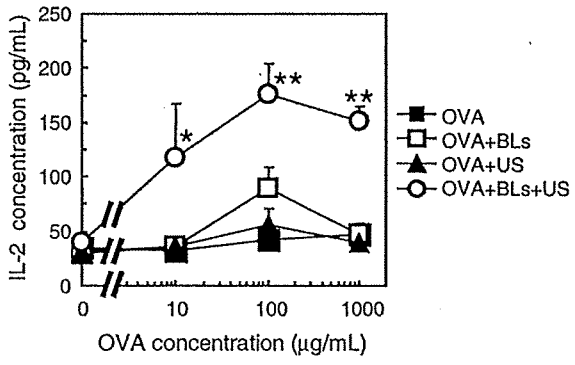

Fig. 2. MHC class I restricted OVA presentation after OVA delivery into DCs using a combination of BLs and US exposure. DCs were pulsed with OVA alone or OVA in conjunction with US exposure and/or BLs. After US exposure, the DCs were incubated for 1 h at 37 °C, then washed with PBS. After culturing for 24 h, the DCs were co-cultured with CD8-OVA1.3 cells for 20 h. The concentration of IL-2 in the supernatants was measured. Each data represents the mean±S.D. for triplicate measurements. *$P<0.05$ compared to the group treated with BLs or US, or without BLs and US. **$P<0.01$ compared to the group treated with BLs or US, or without BLs and US.

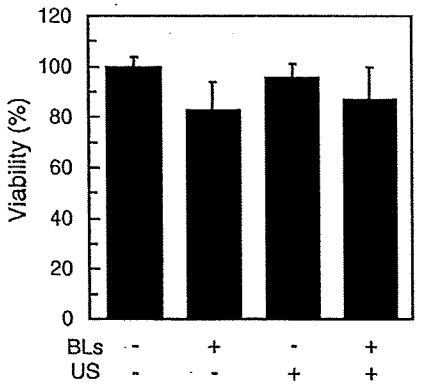

Fig. 3. Viability of DCs treated with BLs and /or US exposure. DCs were treated with BLs and/or US. After US exposure, DCs were incubated for 1 h at 37 °C, then washed with PBS. After culturing for 48 h, the viability of DCs was measured by MTT assay. Each data represents the mean±S.D. for triplicate measurements.

performed using the syngeneic lymphoma cell line EL-4 or its OVA transfectant, E.G7-OVA. As shown in Fig. 4, immunization with DCs without OVA, DCs pulsed with OVA, or OVA combined with BLs or US exposure, induced weak cytotoxicity of splenocytes against the OVA-expressing cell line E.G7-OVA. In contrast, immunization with DCs pulsed with OVA following BL and US exposure resulted in strong cytotoxicity against the OVA-expressing cell line E.G7-OVA by splenocytes. Splenocytes from mice immunized with DCs pulsed using any method of antigen delivery did not exhibit strong cytotoxicity against the parental cell line EL-4. These data indicate that DCs pulsed with antigen using BLs and US exposure as the antigen delivery method efficiently present peptides on MHC class I molecules, which results in strong induction of antigen-specific CTLs *in vivo*.

3.5. Antitumor effects in the immunization of DCs pulsed with antigen by BLs and US exposure

Using an E.G7-OVA tumor model, we examined whether the strong induction of CTLs by antigen delivery with BLs and US exposure leads to efficient anti-tumor immune responses *in vivo*. We immunized C57BL/6 mice twice with bone marrow-derived DCs that had been pulsed using one of two methods of antigen delivery (OVA with US exposure, or OVA with BLs and US exposure). One week after the second immunization, the mice were inoculated intradermally with E.G7-OVA cells, and tumor growth was monitored. As shown in Fig. 5(a) and (b), immunization with untreated DCs weakly suppressed tumor growth. The survival rate of mice immunized with untreated DCs was slightly prolonged, suggesting that non-specific inflammatory responses induced by the injection of DCs result in weak anti-tumor immune responses. Immunization with DCs that had been pulsed with OVA using US exposure suppressed tumor growth slightly more efficiently than the control immunization. Of note, immunization with DCs that had been pulsed with OVA using BLs and US exposure completely suppressed tumor growth, with all mice in this group surviving more than 70 days after tumor inoculation. In addition, we examined the prevention of tumor growth recurrence after re-inoculation of tumor cells into mice, which had completely rejected the first injection of tumor cells (Fig. 5(c)). All mice, which were re-inoculated with E.G7-OVA cells 10 weeks after the first inoculation, completely rejected the tumor cells.

Finally, we examined whether immunization with DCs pulsed with antigen using BLs and US exposure can efficiently suppress the growth of established tumors. For this purpose, we inoculated C57BL/6 mice with E.G7-OVA, and after 9 and 12 days, when the tumors were between 100–200 mm^3, DCs were injected intradermally. As shown in Fig. 6(a), administration of untreated DCs did not provide a significant therapeutic effect. Administration of DCs pulsed with OVA using US exposure exhibited a weak therapeutic effect. Importantly, administration of DCs pulsed with OVA using BLs and US exposure exhibited stronger therapeutic effects in two of the five mice, with these two mice surviving for more than 60 days (Fig. 6(b)). These data indicate that antigen delivery into DCs with BLs and US exposure can induce significant therapeutic effects on established tumors.

4. Discussion

Subunit vaccines utilizing MHC class I-binding peptides have significant limitations that hinder their application to the general patient population (restrictions of HLA types) and that also affect their clinical effectiveness (monovalency of tumor specific antigen) in DC-based tumor immunotherapy. Utilization of tumor associated proteins as antigens may overcome this limitation, thereby enabling a broad spectrum of peptide presentation. In fact, patients treated with tumor cell lysates pulsed DCs showed better response rates compared with patients treated with peptide pulsed DCs [40]. This clinical trial suggests that tumor lysates are a good source of tumor antigens for a polyvalent antitumor vaccine. On the other hand, MHC class I molecules generally present endogenous antigens, whereas exogenous antigens for DCs are taken up by the endocytosis pathway and exogenous antigen-derived peptides are presented on MHC class II molecules [3]. In this study, we showed that by using a combination of BLs and US exposure, exogenous antigen was directly delivered into the cytosol of DCs (Fig. 1) and was presented on MHC class I molecules (Fig. 2). In addition, DCs immunized with antigen delivered by BLs and US exposure could stimulate antigen-specific CTL activation (Fig. 4) and resulted in inducing effective anti-tumor immune responses in tumor-bearing mice. (Figs. 5 and 6) Although peptide and protein delivery with sonoporation using microbubbles have been previously reported [28,29,41], the present study is the first report of effective antigen delivery into DCs by BLs using sonoporation for cancer immunotherapy.

Sonoporation and microbubbles such as Optison have been reported to be an effective gene delivery method using non-viral vectors. In addition, peptide and protein delivery with microbubbles and US exposure has been reported [28,29,41]. In the reports, Bekeredjian et al. showed the feasibility of microbubbles and US exposure for delivery of bioactive protein (luciferase, 60 kDa) into the cytosol of *in vitro* and *in vivo* cells [28,29]. Larina I.V. et al. reported that FITC-dextrans of 10–2000 kDa were delivered into human breast

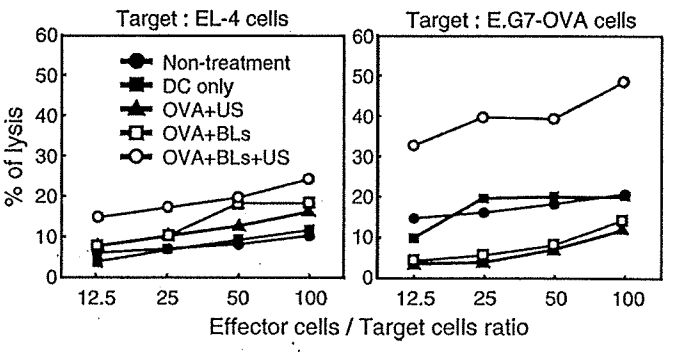

Fig. 4. Antigen specific CTL induction after immunization with DCs treated with BLs and US exposure. DCs were pulsed with OVA under each condition and cultured. After washing the cells, the DCs were intradermally injected into the backs of C57BL/6 mice. After 7 days, the mice were re-immunized. Seven days after the second immunization, splenocytes were obtained and stimulated with mitomycin C-treated E.G7-OVA cells at a ratio of 10:1 for 5 days. The stimulated splenocytes were used as effector cells for a cytotoxicity assay, using EL-4 or E.G7-OVA cells as the target in a flow cytometric assay.

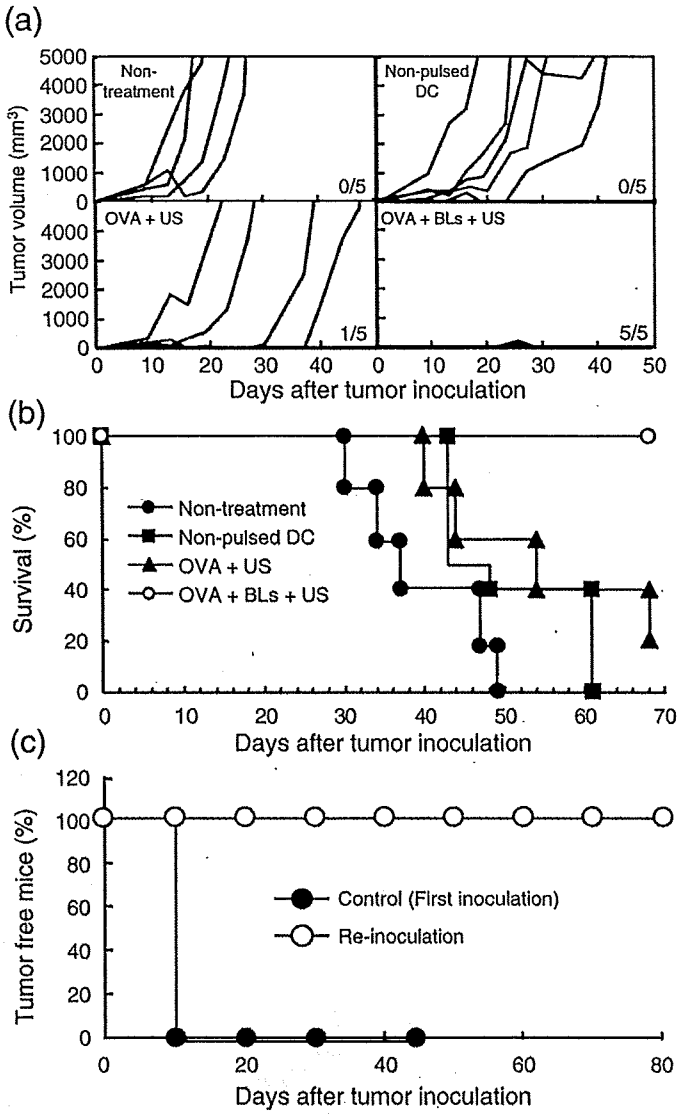

Fig. 5. Antitumor effect caused by immunization of DCs treated with antigen, BLs and US exposure. C57BL/6 mice were immunized with DCs twice. Seven days after the second immunization, E.G7-OVA cells were intradermally inoculated into the backs of the mice, and the tumor volume and survival of the mice was monitored. (a): Tumor volume of the mice after tumor inoculation. Each line indicates the tumor volume in an individual mouse. The fractional number in the lower right of each group shows the number of mice completely rejecting tumors / the number of total experimental mice. (b): Survival rate of the mice after tumor inoculation. (c): Tumor rejection efficiency after re-inoculation with tumor cells. E.G7-OVA cells were re-injected into the mice, which had rejected tumor cells following immunization with DCs treated with OVA, BLs and US in a prior immunization (a). Normal mice were used as controls to confirm the development of cancer following the first inoculation with E.G7-OVA cells. All treated groups contained five mice.

adenocarcinoma (MCF7) by the combination of Optison (conventional microbubbles) and US exposure [42]. It is believed that the delivery mechanism is due to the presence of transient pores through the cell membrane, resulting in extracellular molecules being directly delivered into the cytosol [22,43]. As shown in Fig. 1(b), antigen was directly delivered into DCs by the combination of BLs and US exposure even when the endocytosis pathway was inhibited. Therefore, it is thought that the antigen delivery mechanism induced by BLs and sonoporation is the same as that induced by microbubbles and sonoporation. In studies using microbubbles and sonoporation, pore sizes (based on the physical diameter of the component compounds) were typically between 30–100 nm, and estimates of the membrane recovery time ranged from a few seconds to a few minutes [44]. On the other hand, in studies on the aftereffects of US exposure on cell membranes, Eshet *et al.* reported that microbubbles resulted in a rougher cell surface characterized by depressions, but that the effects are reversible within 24 h following US exposure [43]. In the present study, DCs were incubated with antigen for 1 h after US exposure and increased the delivery efficiency of antigen into the cytosol of DCs. We confirmed the efficiency of MHC class I antigen presentation in DCs with/without 1 h incubation after US exposure. The efficiency following 1 h incubation was higher than that without incubation (data not shown). This result suggests that the membrane permeability of DCs increases even after US exposure. Although the mechanism behind antigen delivery by BLs is unknown, our data support a temporary increase in permeability of the plasma membrane after US exposure. Moreover, recent data from microbubble studies suggest that the resealing of US-induced pores is an energy-dependent process, with the cells exhibiting morphological features consistent with an active and vesicle-based wound-healing responses [45]. Therefore, cells treated with sonoporation are viable due to this recovery mechanism. In this study, the viability of the DCs treated with BLs and US exposure was maintained more than 85% (Fig. 3). The accumulated evidence suggests that the combination of BLs and US exposure is an unique antigen delivery system which can deliver exogenous antigens into the cytosol without serious damage to DCs.

In this study, exogenous antigens, directly delivered into the cytosol of DCs by means of BLs and US exposure, were presented on MHC class I molecules. In addition, immunization of DCs treated with antigen, BLs and US exposure effectively primed antigen-specific CTLs. On the other hand, MHC class I antigen presentation lead to low-level

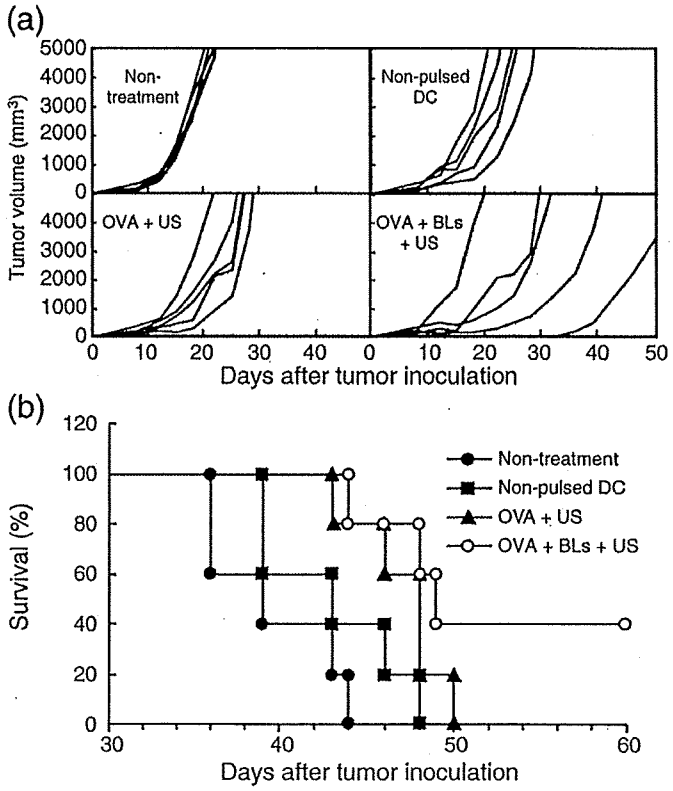

Fig. 6. Immunization of DCs treated with antigen, BLs and US exposure: therapeutic effect on tumor growth. E.G7-OVA cells were intradermally inoculated into the backs of C57BL/6 mice. On day 9, at a tumor size of 8–10 mm, OVA pulsed DCs were intradermally injected into the backs of the mice. On day 12, DCs were injected similarly. The tumor volume and survival of the mice was monitored. (a): Tumor volume of the mice after tumor inoculation. Each line indicates the tumor volume in individual mice. (b): Survival rate of the mice after tumor inoculation. All treated groups contained five mice.

antigen delivery with either BLs or US exposure. In these treated cells, antigen was mainly taken up via the endocytosis pathway. Although we have not confirmed MHC class II presentation, the antigen would presumably be presented on MHC class II molecules to DCs via the general antigen processing mechanism [10]. The exogenous antigens directly delivered into the cytosol would be processed similarly endogenously derived antigens, which are enzymatically digested into peptides, mainly by cytosolic proteases called proteasomes, and are then transported by transporters associated with antigen processing (TAP) molecules into the endoplasmic reticulum (ER). In the ER lumen, peptides bind to MHC class I molecules, which are subsequently transported via the Golgi apparatus to the cell surface [46]. Moreover, immunization of DCs treated with OVA, BLs and US exposure could prime OVA-specific CTLs. This result indicates that DCs presented with OVA-derived epitope peptides on MHC class I molecules effectively prime OVA-specific CTLs *in vivo*. We suspected that the effective priming of antigen-specific CTLs would result in the rejection of tumor cells. As shown in Fig. 5(a), all the immunized mice completely rejected the inoculated tumor cells. Tumor cells were intradermally re-injected into these mice to re-challenge their immune system and assess the preventive effects of immunization for suppressing tumor regeneration (Fig. 5(c)). Rejection following re-challenge with tumor cells suggests the induction of an antigen memory system in the host's immune system, i.e., memory T cells for the immunization antigen. Thus, this therapeutic method has potential for suppressing the regeneration and metastasis of tumors. Finally, we also assessed the therapeutic effects of this treatment towards established tumors (Fig. 6). Immunization with DCs treated with antigen, BLs and US exposure lead to significant therapeutic effects towards established tumors. Tumor cells generally secrete cytokines such as TGF-β to suppress the host's immune system. It is therefore possible that antigen delivery with BLs and US exposure could effectively induce an anti-tumor immune response even in the presence of established tumors.

In conclusion, we have developed a novel system for delivering antigens into DCs using BLs and sonoporation. Immunization of DCs using this antigen delivery system could effectively prime the anti-tumor immune system due to the induction of MHC class I TAA presentation. Therefore, BLs in conjunction with sonoporation might be a useful antigen delivery system for DC-based cancer immunotherapy. In the future, this system will be applied to various antigens containing unknown TAAs, such as crude antigens separated from surgically-removed human tumors.

Acknowledgments

The authors thank Mr. Shota Otake, Mr. Norihito Nishiie, Mr. Ken Osawa, Ms. Risa Koshima, Ms. Motoka Kawamura, Mr. Ryo Tanakadate, Mr. Kunihiko Matsuo and Mr. Yasuyuki Shiono (Teikyo University) for their technical assistance, and Mr. Yasuhiko Hayakawa, Mr. Takahiro Yamauchi and Mr. Kosho Suzuki (Nepa Gene Co., Ltd.) for their technical advice regarding US exposure. This study was supported by the Program for Promotion of Fundamental Studies in Health Sciences of the National Institute of Biomedical Innovation (NIBIO). Tetsuya Kodama acknowledges the Grant for Research on Nanotechnical Medical, the Ministry of Health, Labour and Welfare of Japan (H19-nano-010).

References

[1] F.O. Nestle, A. Farkas, C. Conrad, Dendritic-cell-based therapeutic vaccination against cancer, Curr. Opin. Immunol. 17 (2005) 163–169.
[2] J. Copier, A. Dalgleish, Overview of tumor cell-based vaccines, Int. Rev. Immunol. 25 (2006) 297–319.
[3] R.N. Germain, MHC-dependent antigen processing and peptide presentation: providing ligands for T lymphocyte activation, Cell 76 (1994) 287–299.
[4] P. Elamanchili, M. Diwan, M. Cao, J. Samuel, Characterization of poly(D,L-lactic-co-glycolic acid) based nanoparticulate system for enhanced delivery of antigens to dendritic cells, Vaccine 22 (2004) 2406–2412.
[5] T. Yoshikawa, N. Okada, A. Oda, K. Matsuo, K. Matsuo, Y. Mukai, Y. Yoshioka, T. Akagi, M. Akashi, S. Nakagawa, Development of amphiphilic gamma-PGA-nanoparticle based tumor vaccine: potential of the nanoparticulate cytosolic protein delivery carrier, Biochem. Biophys. Res. Commun. 366 (2008) 408–413.
[6] P. Machy, K. Serre, L. Leserman, Class I-restricted presentation of exogenous antigen acquired by Fcgamma receptor-mediated endocytosis is regulated in dendritic cells, Eur. J. Immunol. 30 (2000) 848–857.
[7] N. Okada, T. Saito, K. Mori, Y. Masunaga, Y. Fujii, J. Fujita, K. Fujimoto, T. Nakanishi, K. Tanaka, S. Nakagawa, T. Mayumi, T. Fujita, A. Yamamoto, Effects of lipofectin-antigen complexes on major histocompatibility complex class I-restricted antigen presentation pathway in murine dendritic cells and on dendritic cell maturation, Biochim. Biophys. Acta 1527 (2001) 97–101.
[8] L. Wang, H. Ikeda, Y. Ikuta, M. Schmitt, Y. Miyahara, Y. Takahashi, X. Gu, Y. Nagata, Y. Sasaki, K. Akiyoshi, J. Sunamoto, H. Nakamura, K. Kuribayashi, H. Shiku, Bone marrow-derived dendritic cells incorporate and process hydrophobized polysaccharide/oncoprotein complex as antigen presenting cells, Int. J. Oncol. 14 (1999) 695–701.
[9] K. Kawamura, N. Kadowaki, R. Suzuki, S. Udagawa, S. Kasaoka, N. Utoguchi, T. Kitawaki, N. Sugimoto, N. Okada, K. Maruyama, T. Uchiyama, Dendritic cells that endocytosed antigen-containing IgG-liposomes elicit effective antitumor immunity, J. Immunother. 29 (2006) 165–174.
[10] K.W. Kim, S.H. Kim, J.H. Jang, E.Y. Lee, S.W. Park, J.H. Um, Y.J. Lee, C.H. Lee, S. Yoon, S.Y. Seo, M.H. Jeong, S.T. Lee, B.S. Chung, C.D. Kang, Dendritic cells loaded with exogenous antigen by electroporation can enhance MHC class I-mediated antitumor immunity, Cancer Immunol. Immunother. 53 (2004) 315–322.
[11] J.M. Weiss, C. Allen, R. Shivakumar, S. Feller, L.H. Li, L.N. Liu, Efficient responses in a murine renal tumor model by electroloading dendritic cells with whole-tumor lysate, J. Immunother. 28 (2005) 542–550.
[12] M. Fechheimer, J.F. Boylan, S. Parker, J.E. Sisken, G.L. Patel, S.G. Zimmer, Transfection of mammalian cells with plasmid DNA by scrape loading and sonication loading, Proc. Natl. Acad. Sci. U. S. A. 84 (1987) 8463–8467.
[13] M.W. Miller, D.L. Miller, A.A. Brayman, A review of in vitro bioeffects of inertial ultrasonic cavitation from a mechanistic perspective, Ultrasound Med. Biol. 22 (1996) 1131–1154.
[14] M. Joersbo, J. Brunstedt, Protein synthesis stimulated in sonicated sugar beet cells and protoplasts, Ultrasound Med. Biol. 16 (1990) 719–724.
[15] D.L. Miller, S.V. Pislaru, J.E. Greenleaf, Sonoporation: mechanical DNA delivery by ultrasonic cavitation, Somat. Cell Mol. Genet. 27 (2002) 115–134.
[16] H.R. Guzman, A.J. McNamara, D.X. Nguyen, M.R. Prausnitz, Bioeffects caused by changes in acoustic cavitation bubble density and cell concentration: a unified explanation based on cell-to-bubble ratio and blast radius, Ultrasound Med. Biol. 29 (2003) 1211–1222..
[17] W. Wei, B. Zheng-zhong, W. Yong-jie, Z. Qing-wu, M. Ya-lin, Bioeffects of low-frequency ultrasonic gene delivery and safety on cell membrane permeability control, J. Ultrasound Med. 23 (2004) 1569–1582.
[18] H.J. Kim, J.F. Greenleaf, R.R. Kinnick, J.T. Bronk, M.E. Bolander, Ultrasound-mediated transfection of mammalian cells, Hum. Gene Ther. 7 (1996) 1339–1346.
[19] D.B. Tata, F. Dunn, D.J. Tindall, Selective clinical ultrasound signals mediate differential gene transfer and expression in two human prostate cancer cell lines: LnCap and PC-3, Biochem. Biophys. Res. Commun. 234 (1997) 64–67.
[20] M. Duvshani-Eshet, M. Machluf, Therapeutic ultrasound optimization for gene delivery: a key factor achieving nuclear DNA localization, J. Control. Release 108 (2005) 513–528.
[21] W.J. Greenleaf, M.E. Bolander, G. Sarkar, M.B. Goldring, J.F. Greenleaf, Artificial cavitation nuclei significantly enhance acoustically induced cell transfection, Ultrasound Med. Biol. 24 (1998) 587–595.
[22] Y. Taniyama, K. Tachibana, K. Hiraoka, M. Aoki, S. Yamamoto, K. Matsumoto, T. Nakamura, T. Ogihara, Y. Kaneda, R. Morishita, Development of safe and efficient novel nonviral gene transfer using ultrasound: enhancement of transfection efficiency of naked plasmid DNA in skeletal muscle, Gene Ther. 9 (2002) 372–380.
[23] S. Chen, J.H. Ding, R. Bekeredjian, B.Z. Yang, R.V. Shohet, S.A. Johnston, H.E. Hohmeier, C.B. Newgard, P.A. Grayburn, Efficient gene delivery to pancreatic islets with ultrasonic microbubble destruction technology, Proc. Natl. Acad. Sci. U. S. A. 103 (2006) 8469–8474.
[24] A. Aoi, Y. Watanabe, S. Mori, M. Takahashi, G. Vassaux, T. Kodama, Herpes simplex virus thymidine kinase-mediated suicide gene therapy using nano/microbubbles and ultrasound, Ultrasound Med. Biol. 34 (2008) 425–434.
[25] Z.P. Shen, A.A. Brayman, L. Chen, C.H. Miao, Ultrasound with microbubbles enhances gene expression of plasmid DNA in the liver via intraportal delivery, Gene Ther. (2008).
[26] S. Sonoda, K. Tachibana, E. Uchino, A. Okubo, M. Yamamoto, K. Sakoda, T. Hisatomi, K.H. Sonoda, Y. Negishi, Y. Izumi, S. Takao, T. Sakamoto, Gene transfer to corneal epithelium and keratocytes mediated by ultrasound with microbubbles, Investig. Ophthalmol. Vis. Sci. 47 (2006) 558–564.
[27] K. Iwanaga, K. Tominaga, K. Yamamoto, M. Habu, H. Maeda, S. Akifusa, T. Tsujisawa, T. Okinaga, J. Fukuda, T. Nishihara, Local delivery system of cytotoxic agents to tumors by focused sonoporation, Cancer Gene Ther. 14 (2007) 354–363.
[28] R. Bekeredjian, S. Chen, P.A. Grayburn, R.V. Shohet, Augmentation of cardiac protein delivery using ultrasound targeted microbubble destruction, Ultrasound Med. Biol. 31 (2005) 687–691.
[29] R. Bekeredjian, H.F. Kuecherer, R.D. Kroll, H.A. Katus, S.E. Hardt, Ultrasound-targeted microbubble destruction augments protein delivery into testes, Urology 69 (2007) 386–389.
[30] T. Yamashita, S. Sonoda, R. Suzuki, N. Arimura, K. Tachibana, K. Maruyama, T. Sakamoto, A novel bubble liposome and ultrasound-mediated gene transfer to ocular surface: RC-1 cells in vitro and conjunctiva in vivo, Exp. Eye Res. 85 (2007) 741–748.

[31] R. Suzuki, T. Takizawa, Y. Negishi, K. Hagisawa, K. Tanaka, K. Sawamura, N. Utoguchi, T. Nishioka, K. Maruyama, Gene delivery by combination of novel liposomal bubbles with perfluoropropane and ultrasound, J. Control. Release 117 (2007) 130–136.
[32] R. Suzuki, T. Takizawa, Y. Negishi, N. Utoguchi, K. Maruyama, Effective gene delivery with novel liposomal bubbles and ultrasonic destruction technology, Int. J. Pharm. 354 (2008) 49–55.
[33] R. Suzuki, T. Takizawa, Y. Negishi, N. Utoguchi, K. Sawamura, K. Tanaka, E. Namai, Y. Oda, Y. Matsumura, K. Maruyama, Tumor specific ultrasound enhanced gene transfer in vivo with novel liposomal bubbles, J. Control. Release 125 (2008) 137–144.
[34] R. Suzuki, T. Takizawa, Y. Negishi, N. Utoguchi, K. Maruyama, Effective gene delivery with liposomal bubbles and ultrasound as novel non-viral system, J. Drug Target. 15 (2007) 531–537.
[35] J.D. Pfeifer, M.J. Wick, R.L. Roberts, K. Findlay, S.J. Normark, C.V. Harding, Phagocytic processing of bacterial antigens for class I MHC presentation to T cells, Nature 361 (1993) 359–362.
[36] K. Inaba, M. Inaba, M. Deguchi, K. Hagi, R. Yasumizu, S. Ikehara, S. Muramatsu, R.M. Steinman, Granulocytes, macrophages, and dendritic cells arise from a common major histocompatibility complex class II-negative progenitor in mouse bone marrow, Proc. Natl. Acad. Sci. U. S. A. 90 (1993) 3038–3042.
[37] D.P. Guo, X.Y. Li, P. Sun, Y.B. Tang, X.Y. Chen, Q. Chen, L.M. Fan, B. Zang, L.Z. Shao, X.R. Li, Ultrasound-targeted microbubble destruction improves the low density lipoprotein receptor gene expression in HepG2 cells, Biochem. Biophys. Res. Commun. 343 (2006) 470–474.
[38] T. Mosmann, Rapid colorimetric assay for cellular growth and survival: application to proliferation and cytotoxicity assays, J. Immunol. Methods 65 (1983) 55–63.
[39] S.E. Slezak, P.K. Horan, Cell-mediated cytotoxicity. A highly sensitive and informative flow cytometric assay, J. Immunol. Methods 117 (1989) 205–214.
[40] G. Reinhard, A. Marten, S.M. Kiske, F. Feil, T. Bieber, I.G. Schmidt-Wolf, Generation of dendritic cell-based vaccines for cancer therapy, Br. J. Cancer 86 (2002) 1529–1533.
[41] M. Kinoshita, K. Hynynen, Intracellular delivery of Bak BH3 peptide by microbubble-enhanced ultrasound, Pharm. Res. 22 (2005) 716–720.
[42] I.V. Larina, B.M. Evers, R.O. Esenaliev, Optimal drug and gene delivery in cancer cells by ultrasound-induced cavitation, Anticancer Res. 25 (2005) 149–156.
[43] M. Duvshani-Eshet, D. Adam, M. Machluf, The effects of albumin-coated microbubbles in DNA delivery mediated by therapeutic ultrasound, J. Control. Release 112 (2006) 156–166.
[44] C.M. Newman, T. Bettinger, Gene therapy progress and prospects: ultrasound for gene transfer, Gene Ther. 14 (2007) 465–475.
[45] R.K. Schlicher, H. Radhakrishna, T.P. Tolentino, R.P. Apkarian, V. Zarnitsyn, M.R. Prausnitz, Mechanism of intracellular delivery by acoustic cavitation, Ultrasound Med. Biol. 32 (2006) 915–924.
[46] P.M. Kloetzel, Antigen processing by the proteasome, Nat. Rev. Mol. Cell. Biol. 2 (2001) 179–187.

NANOMEDICINE

Journal of Controlled Release 140 (2009) 306–311

Contents lists available at ScienceDirect

Journal of Controlled Release

journal homepage: www.elsevier.com/locate/jconrel

Enhanced magnetic resonance imaging of experimental pancreatic tumor *in vivo* by block copolymer-coated magnetite nanoparticles with TGF-β inhibitor

Michiaki Kumagai [a,e,1], Mitsunobu R. Kano [b,f,1], Yasuyuki Morishita [b], Motomi Ota [a], Yutaka Imai [a], Nobuhiro Nishiyama [a,e,f], Masaki Sekino [c], Shoogo Ueno [d], Kohei Miyazono [b,f], Kazunori Kataoka [a,e,f,*]

[a] Department of Materials Engineering, Graduate School of Engineering, The University of Tokyo, 7-3-1 Hongo, Bunkyo-ku, Tokyo 113-8656, Japan
[b] Department of Molecular Pathology, Graduate School of Medicine, The University of Tokyo, 7-3-1 Hongo, Bunkyo-ku Tokyo 113-0033, Japan
[c] Department of Advanced Energy, Graduate School of Frontier Sciences, The University of Tokyo, 5-1-5, Kashiwanoha, Kashiwa-shi, Chiba, 277-8561, Japan
[d] Department of Applied Quantum Physics, Graduate School of Engineering, Kyushu University, 6-10-1 Hakozaki, Higashi-ku Fukuoka 812-8581, Japan
[e] Center for Disease Biology and Integrative Medicine, School of Medicine, The University of Tokyo, 7-3-1 Hongo, Bunkyo-ku, Tokyo 113-0033, Japan
[f] Center for NanoBio Integration, The University of Tokyo, 7-3-1 Hongo, Bunkyo-ku, Tokyo 113-8656, Japan

ARTICLE INFO

Article history:
Received 13 March 2009
Accepted 5 June 2009
Available online 12 June 2009

Keyword:
Magnetic resonance imaging
Pancreatic cancer
TGF-β
Magnetite nanoparticles
Poly(ethylene glycol)

ABSTRACT

Early detection of solid tumors, particularly pancreatic cancer, is of substantial importance in clinics. Enhanced magnetic resonance imaging (MRI) with iron oxide nanoparticles is an available way to detect the cancer. The effective and selective accumulation of these nanoparticles in the tumor tissue is needed for improved imaging, and in this regard, their longevity in the blood circulation time is crucial. We developed here block copolymer-coated magnetite nanoparticles for pancreatic cancer imaging, by means of a chelation between the carboxylic acid groups in poly(ethylene glycol)–poly(aspartic acid) block copolymer (PEG–PAsp) and Fe on the surface of the iron oxide nanoparticles. These nanoparticles had considerably narrow distribution, even upon increased ionic strength or in the presence of fetal bovine serum. The PEG–PAsp-coated nanoparticles were further shown to be potent as a contrast agent for enhanced MRI for an experimental pancreatic cancer, xenografts of the human-derived BxPC3 cell line in BALB/c nude mice, with combined administration of TGF-β inhibitor. Iron staining of tumor tissue confirmed the accumulation of the nanoparticles in tumor tissue. Use of the PEG–PAsp-coated magnetite nanoparticles, combined with the TGF-β inhibitor, is of promising clinical importance for the detection of intractable solid cancers, including pancreatic cancer.

1. Introduction

Pancreatic cancer, one of the intractable solid tumors, is the fourth leading cause of cancer-related deaths in the United States and the fifth in Japan [1]. The average survival period of patients suffering from advanced pancreatic adenocarcinoma is still extremely short, only 6 months, despite recent progress in the chemotherapies [2]. Although cancer detection and treatment have been greatly improved through the development of diagnostic imaging modalities, it is still difficult to detect pancreatic cancer [3]. Consequently, the development of diagnostic systems to detect these cancers is of great importance.

Recently, superparamagnetic iron oxide (SPIO) nanoparticles composed of either magnetite (Fe_3O_4) or maghemite (g-Fe_2O_3) have been studied as contrast agents for magnetic resonance (MR) imaging [4]. Commercial application for human diagnosis based on SPIO particles is currently available. However, since cancer detection requires the systemic administration of iron oxide nanoparticles, the circulation time of the particles must be prolonged. Several studies have already reported that the behavior of magnetic nanoparticles in the bloodstream depends closely on their nanoscale morphology, including overall diameter, size distribution, or nature of the surface [5,6]. Additionally, the surface modification of iron oxide nanoparticles has proved a versatile strategy for improving their biological performance, including the reduction of immunogenicity and enhancement of targeted delivery to specific tissues [7]. However, the overall correlation between the surface modification of nanoparticles and their *in vivo* behavior remains to be further elucidated.

Various methods of stabilization for SPIO nanoparticles have been reported to date [8]. One of the most feasible approaches could be the stabilization of SPIO by coated with biocompatible polymers [9]. Suitable polymers, including poly(ethylene glycol) (PEG) and its block copolymers, are promising for the development of SPIO systems with defined surface properties. This coating of particles with PEG, or PEGylation, to avoid their uptake by the reticuloendothelial system, is under intensive investigation. We also previously reported the accumulation of β-FeOOH nanoparticles coated with PEG–poly(α,β-aspartic acid) block copolymer

* Corresponding author. Department of Materials Engineering, Graduate School of Engineering, The University of Tokyo, 7-3-1 Hongo, Bunkyo-ku, Tokyo 113-8656, Japan.
E-mail address: kataoka@bmw.t.u-tokyo.ac.jp (K. Kataoka).
[1] Equal contribution.

0168-3659/$ – see front matter © 2009 Elsevier B.V. All rights reserved.
doi:10.1016/j.jconrel.2009.06.002